PRESSURE RETARDED OSMOSIS FOR ENERGY RECOVERY FROM HIGH SALINITY WATERS

A Thesis

by

AMEEN AHMAD SIDDIQUI

Submitted to the Office of Graduate and Professional Studies of
Texas A&M University
in partial fulfillment of the requirements for the degree of

MASTER OF SCIENCE

Chair of Committee,	Ahmed Abdel-Wahab
Co-Chair of Committee,	Mahmood Amani
Committee Member,	Hamid Parsaei
Head of Department,	Arul Jayaraman

August 2020

Major Subject: Chemical Engineering

ABSTRACT

The demand for energy is increasing every year, with more people being added to the world energy network due to global development. The global access to electricity has increased over the past two decades. The areas previously having little or no access to electricity are rapidly getting access to modes of power consumption. All this and growing world population is putting a heavy toll on already depleting conventional sources of energy. The majority of electricity worldwide is still produced using oil, gas, and coal. But with increased environmental awareness, non-conventional sources of clean energy are being rapidly developed.

Osmotic power is one such non-conventional source of power. It uses the saline energy difference between two solutions to produce power. The technology employed to harness osmotic power is known as Pressure Retarded Osmosis or PRO.

PRO is a membrane-based technology that uses a semi-permeable membrane to selectively allow water molecules to pass through it but prevents the exchange of solute molecules. It was developed by Sidney Loeb in the year 1973.

In this research, PRO utility is experimentally determined using flat sheet membranes. The bench-scale setup was constructed and based on experimental findings on this setup, optimum condition for the efficient performance of a PRO system is predicted i.e. appropriate feed and draw solutions compositions, transmembrane pressure difference, and optimal support and spacers.

The membrane selection for the experiment was determined based on the intrinsic transport characteristics A (Pure water permeability, L m^{-2} h^{-1} bar^{-1}), B (Salt permeability, L m^{-2} h^{-1}), and S (Structural parameter, microns). Of the two commercial membranes thin film-composite (TFC) and FTS cellulose tri-acetate (CTA) used in this study, the TFC membranes showed better water permeability but they cannot withstand high-pressure load and failed at 35 bar. The CTA membrane, though having lower water permeability were able to work till 55 bar of pressure. But on using the tricot spacers and modified support plate the CTA membrane produced higher water flux and maximum power density of 19 W/m^2 at 30 bar of transmembrane pressure.

ACKNOWLEDGEMENTS

I would like to express my thanks and deepest gratitude to my committee comprising of Dr. Ahmed Abdel-Wahab, Dr. Mahmood Amani, and Dr. Hamid Parsaei. I am extremely grateful to Dr. Ahmed Abdel-Wahab and Dr. Mahmood Amani who presented me with an opportunity to work on this exciting project and provided me the resources to learn and grow as a researcher. I would also like to thank Dr. Hamid Parsaei for his continuous guidance and mentorship.

I am also thankful to Dr. Khaled Elsaid who helped me with brainstorming and in the designing of the experiments. I would also like to express my gratitude to Marcin Kozusznik for providing those invaluable lessons with tools, machines, and various software. It was due to him the construction and smooth operation of the PRO setup was possible.

Special thanks to all my friends and colleagues at Texas A and M University at Qatar for being supportive throughout my journey of graduate studies.

Finally, I would like to express my love and gratitude for my family especially my beloved parents for always praying for my wellbeing and keeping me motivated in finishing my M.S. degree.

CONTRIBUTORS AND FUNDING SOURCES

Contributors

This work was supervised by a thesis committee comprising of Professor Ahmed Abdel-Wahab (Chair) of the Department of Chemical Engineering and Professor Mahmood Amani (Co-chair) of the Department of Petroleum Engineering and Professor Hamid Parsaei (Member) of the Department of Industrial and Systems Engineering.

The Equation of State for the theoretical calculation of the osmotic pressure in Chapter 4 was provided by Husnain Manzoor.

All other work conducted for the thesis was completed by the student independently.

Funding Sources

This work was made possible in part by the National Priorities Research Program (NPRP) of Qatar National Research Fund under Grant Number NPRP10-1231-160069 and in part by the ConocoPhillips Global Water Sustainability Center (GWSC).

Its contents are solely the responsibility of the authors and do not necessarily represent the official views of the sponsors.

NOMENCLATURE

a_w	Water activity value
A	Water permeability coefficient
A_m	Available membrane area
b	Molality
B	Salt permeability coefficient
C	Concentration of the solution
$C_{D,b}$	Concentration of the draw bulk fluid
$C_{D,m}$	Concentration of the draw fluid at the membrane surface.
$C_{F,b}$	Concentration of the feed bulk fluid
$C_{F,m}$	Concentration of the feed fluid at the membrane surface
c_p	Concentration of the permeate
d_h	Hydraulic diameter
D	Diffusivity coefficient
F	Faraday's constant
ΔG	Gibb's free energy of mixing
h	Total waters of hydration per mole of solute
i	vant's Hoff factor
J_w	Water flux
J_s	Salt flux
k	Mass transfer coefficient

K	Solute resistivity
L	Length of a flow channel
Δm	Mass change
M	Molarity
M_w	Mass of water
n_s	Number of moles of solute
P	Transmembrane or Hydraulic Pressure
P_s	Pressure of solvent in the solution
R	Universal gas constant
Re	Reynolds number
S	Structural parameter
Sc	Schmidt number
Sh	Sherwood number
t	Time
v_{H2O}	Molar volume of water
W	Power density
z	Ionic charge

Greek Letters

v	Flow velocity
ρ	Density
π	Osmotic pressure

η	Dynamic viscosity
μ	Kinematic viscosity
λ_i	Ionic equivalent conductance
φ	Fugacity coefficient
ϕ	Feed fraction

Abbreviations

FO	Forward osmosis
RO	Reverse osmosis
PRO	Pressure retarded osmosis
SGE	Salinity gradient energy
CP	Concentration polarization
ICP	Internal concentration polarization
ECP	External concentration polarization
NSTD	Normalized standard deviation
UF	Ultrafiltration
LPRO	Low-pressure reverse osmosis
PLA	Poly lactic acid
CTA	Cellulose tri-acetate
TFC	Thin film-composite
FTS	Fluid technology solutions
TMP	Transmembrane pressure

TABLE OF CONTENTS

Page

LIST OF FIGURES

Page

LIST OF TABLES

Page

1. INTRODUCTION

The fast pace of global development accompanied by increasing population has led to growth in demand for energy, especially in the past 50 years for all major sectors such as residential, agriculture, industrial, and transport. The energy required is mainly sourced using fossil fuels, which are also the primary source of greenhouse gases (GHGs). The emission of greenhouse gases have numerous adverse impact such as climate change, melting of polar ice caps, wildfire, and an increase in floods [1]. Along with the environmental concerns, the availability of fossil fuels in the future and waste generated due to its production is also raising concerns and have forced mankind to look for alternative sources of energy. The exploration of clean, affordable, efficient, and substantial energy sources is still a challenge for countries all around the globe. With energy security becoming a priority for global economies, the pace for development of new energy sources is on the increase. The major non- conventional energy sources such as solar, wind, tidal, geothermal, and biomass are being commercially employed around the world. Other than these, other sources of energy that are in the development stage include salinity gradient energy which uses the osmotic pressure of the saline solutions to produce energy.

The salinity gradient energy (SGE) of saline solutions is harnessed using Pressure Retarded Osmosis (PRO) technology. PRO is a membrane-based technology that converts the chemical energy to mechanical energy and can be utilized to produce work. The theoretical potential for energy production using SGE is around 647 GW which is 23% of

total electricity consumption in 2011 [2]. Due to its high power generation potential and abundant availability of saline water sources, osmotic power systems are being extensively researched recently.

One of the major sources of saline water is seawater and high salinity produced water obtained from oil and gas wells during their extraction. The Middle East region has substantial availability of both these sources of saline waters, which makes PRO technology an attractive source of alternative energy in the region.

The production of energy using saline water requires efficient PRO systems design, which can only be achieved by using suitable membranes with good performance under different conditions. In this study, flat sheet cellulose tri-acetate and thin-film composite membranes are used in a bench-scale PRO setup. The performance of the membranes is evaluated by determining their ability to produce water flux and power density when using a feed solution of varying concentration against hypersaline draw solution. Also, the intrinsic characteristics of membranes are determined on an RO-FO setup following established procedure [3]. The knowledge of membrane characteristics at the lab scale can be used to predict the membrane performance towards scaling up the PRO technology. The system performance study is also done based on the feed spacer configuration and design, as it is observed having the improved feed spacer design allows us to reach higher power densities and prevent pressure losses in the feed channel. The osmotic pressure of the solution used in the PRO experiments is also determined experimentally using an osmometer.

The thesis consists of five chapters. In chapter one, the introduction and objective of the study are presented. In chapter two, a literature review about the PRO technology is presented. Chapter three includes a detailed description of the methods and materials used for performing the experiments in the lab. Chapter four presents the results and findings of this study. Finally, Chapter five includes conclusions of the study and recommendations for future work scope. The references used in the study are listed after the conclusion.

2. THEORETICAL BACKGROUND

In this chapter the literature review about the membrane technologies with emphasis on PRO membranes, and spacer configurations and draw solutions is presented in detail.

2.1 Osmosis

The movement of a solvent (water, in the case of aqueous media) towards a region of low solute concentration from a region of high solute concentration is defined as osmosis. A low solute concentration solution is called hypotonic, while a highly concentrated solution is called hypertonic. Water/solvent continues to move across the membrane to make the solutions isotonic, i.e., the solute concentrations of both the solutions become equal and they are said to be in equilibrium. The reverse process of osmosis can be employed by applying pressure on the high solute concentration side, which results in solvent movement from high solute concentration side to the low solute concentration side. Osmotic pressure is described as the pressure which is required to stop the natural movement of a solvent through a semi-permeable membrane and prevent further dilution of the concentrated solution. Currently, osmosis processes find their application in various areas, i.e., desalination, drug release technologies, food processing, water treatment, and power generation [4].

There are three types of osmotic processes, i.e., pressure retarded osmosis (PRO), forward osmosis (FO), and reverse osmosis (RO).

Forward osmosis is a technique that uses an osmotic pressure gradient to draw water across the membrane between the concentrated draw solution and the dilute feed solution. The

increased osmotic pressure causes the movement of water from the dilute feed solution towards the concentrated draw solution, resulting in the complete removal of water from the feed solution [4]–[6]. For FO, the osmotic pressure gradient ($\Delta\pi$) > 0, where the hydrostatic pressure (ΔP) = 0 [4], [6].

Reverse osmosis is another technique where hydrostatic pressure is applied to move the solvent towards a low solute concentration region from a high concentration region via a semi-permeable membrane. The hydrostatic pressure applied in reverse osmosis is higher than that of osmotic pressure. For RO, hydrostatic pressure (ΔP) > osmotic pressure gradient ($\Delta\pi$) [4], [6]. If the hydrostatic pressure becomes too high, there is a risk that the solid particles will block the membrane, affecting its performance in an irreversible manner. Also, the hydrostatic pressure will be limited to a certain threshold because of the energy pumping requirements. RO technology is used in most modern desalination plants built all over the world [6].

Pressure retarded osmosis is an intermediate technique between forward and reverse osmosis, where water/solvent moves from a dilute solution (feed) towards a partially pressurized concentrated solution through a semipermeable membrane where the hydrostatic pressure (ΔP) < osmotic pressure ($\Delta\pi$). The movement of water continues from dilute to concentrated solution but flux decreases with time. Consequently, at the pressurized side of the draw solution, the volumetric flow of the solvent increases, and this flow can be used as the energy source at power generation stations [4], [6], [7]. The three types of osmotic phenomena that take place during the process of osmosis are shown in Figure 1.

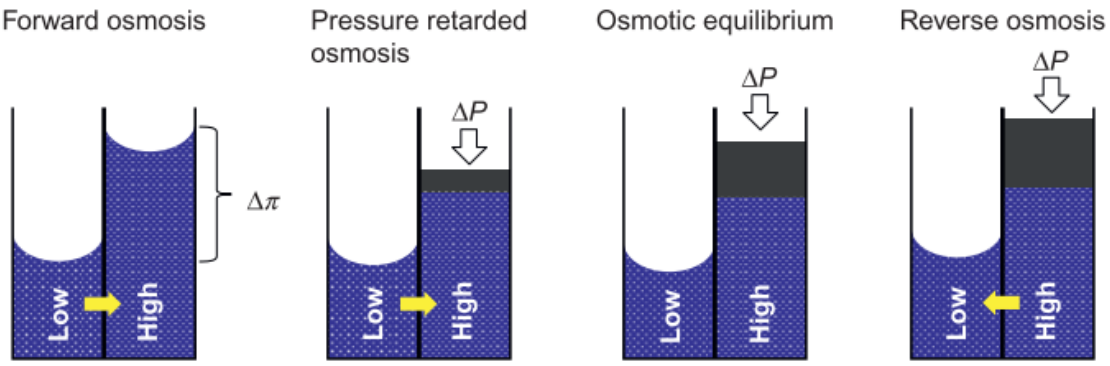

Figure 1: Demonstration of forward, reverse and pressure retarded osmosis, along with the directions of applied force (pressure) on draw and feed solutions[6]**.** [1]

In the early 1980s, Lee et al. characterized the three osmotic processes as forward osmosis when $\Delta P = 0$, reverse osmosis when $\Delta P > \Delta\pi$ and pressure retarded osmosis when $\Delta\pi > \Delta P$. Figure 2 shows the operational parameters, i.e., pressure gradient, water flux and hydrostatic pressure, and the way these parameters relate to each other during FO, RO, and PRO processes. In the case of zero difference of hydrostatic pressure between both side solutions, forward osmosis takes place. However, when the applied pressure difference exceeds that of the osmosis pressure gradient, reverse osmosis takes place. In the case where the applied pressure lies somewhere between the reversal flux point and zero, pressure retarded osmosis takes place.

[1] Reprinted with permission from "Sustainable Energy from Salinity Gradients. Pressure retarded osmosis: Fundamentals. 2016" by S. Zhang, G. Han, X. Li, C. Wan, and T. S. Chung. http:// dx.doi.org/10.1016/B978-0-08-100312-1.00002-X. Copyright © 2016 Elsevier Ltd.

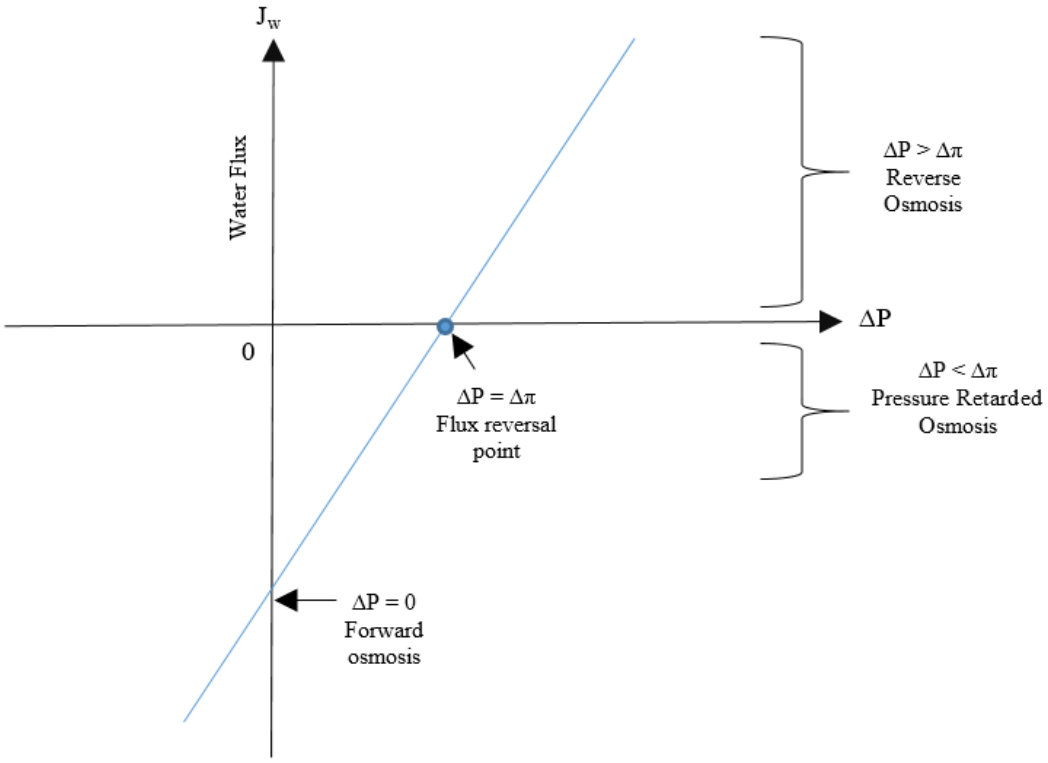

Figure 2: Flux direction and driving force for forward, reverse, and pressure retarded osmosis [8]**.** [2]

2.2 Pressure Retarded Osmosis

The concept of Pressure retarded osmosis or PRO came into existence around the mid-1950s when Pattle published an article in the Nature Journal [9]. The idea of Pattle at that time did not receive much attention from the scientific community and it was only after

[2] Reprinted with permission from "Membranes for power generation by pressure-retarded osmosis," by K. L. Lee, R. W. Baker, and H. K. Lonsdale, 1981, J. Memb. Sci., vol. 8, no. 2, pp. 141–171. Copyright © 1981 Elsevier B.V.

two decades when the oil crisis of 1973 occurred, the interest in PRO revived along with other forms of renewable energy.

From 1974 to 1976, there were four articles published about PRO utilization for power generation [10]–[13]. The schematic diagram of energy converter based on osmosis was proposed by Norman et al. in the year 1974 [13]. In his study, they mentions how freshwater on permeating across the membrane in the pressurized seawater section causes a spill, the pressurized spill can then be used to run a water wheel attached to a generator. In 1975, Sidney Loeb coined the term PRO; Loeb and Norman [12] proposed the osmotically driven membrane process (OMDP) for PRO. Finally, in the year 1976, first experimental results were published by Loeb et al. [11]; in their experiments they employed RO hollow fiber membranes using seawater brine as draw solution and freshwater as feed solution. The success of the experiments helped in establishing the concept of PRO though the results were not very promising, which was due to the utilization of RO membranes.

Based on his previous experiment Loeb along with Mehta put forward the term Internal concentration polarization (ICP) in the year 1978 [14], where they introduced the adverse effect of ICP for power production using PRO. In 1979, the results published by Mehta and Loeb showed PRO as a potential source of renewable energy if proper system design and suitable membrane are employed. In 1981, Lee et al. developed a model incorporating the effects of ICP only in a PRO process for calculating power density and water flux, this model served as a reference for the development of future PRO models [8]. Meanwhile, Loeb et al. [15] continued his research work and studied theoretically the

various design considerations for improving mechanical efficiency of PRO processes. In their study, they concluded that the counter-flow scheme has higher efficiency but it required additional pressure vessels. Also, Reali et al. [16] employed numerical methods for determining the profile of salt concentration in support layer of the membrane thereby demonstrating the importance of membrane intrinsic characteristics namely water permeability coefficient A, the salt permeability coefficient B, and the structural parameter S for given asymmetric membranes.

The research work of Sidney Loeb continued through the first decade of 2000 looking into the feasibility of utilizing hypersaline natural water bodies [17][18]. In the year 2002, Loeb [19] introduced pressure exchangers utilization for PRO systems in order to improve overall net energy output by reducing the power consumption required to pressurize the PRO systems.

In 2009, the commercialization of PRO was attempted by Norwegian company Statkraft when the first PRO pilot plant was built. However, it was stopped in the year 2014 due to economic reasons. The results of the Statkraft plant motivated the scientific community to investigate and address the challenges faced by Statkraft. It was reported by Statkraft for PRO to be commercially viable, PRO units should be able to generate at least 5 W/m^2 of power density. There are numerous lab-scale experimental studies published using flat sheet membranes and reported power densities as high as 59.7 W/m^2 [20]. But the same has not been replicated on a commercial scale yet. Recently, process simulation and optimization models for assessing the techno-economic feasibility of full-scale PRO plant [21]. Research work continues all over the world for enhancing the

efficiency of PRO technology by developing new membranes with enhanced intrinsic properties and/or optimizing process design and configuration.

2.2.1 PRO Theory

i. Water fluidity and Transport for an Ideal Membrane

A membrane is a semi-permeable barrier, allowing certain particles to pass through while restricting the transport of the others. In PRO, the membrane is used to separate the solutions with different salinities from each other. The solution having higher salinity is called a draw solution while the solution with lower salinity is called feed [22].

The mathematical relationship for the water transport and flux across the semipermeable membrane is given as [6], [23], [24]:

$$J_w = A(\Delta\pi - \Delta P) \qquad Eq.(1)$$

where, J_w is water flux, A is pure water permeability, $\Delta\pi$ osmotic pressure gradient and ΔP is the hydraulic pressure difference.

The natural driving force which is required to move water from the feed side o to the draw side of the membrane is described as the osmotic pressure difference. The hydraulic pressure is applied on the draw side [23].

ii. Water fluidity and Transport for a Real Membrane

A real membrane allows solute to diffuse across the membrane layer, this develops a local solute concentration inside the membrane. In reality, water flux will be lower than that described by Eq. (1) due to the diffusion of salt across the membrane. The mathematical notation for the reverse salt flux across the membrane, J_s can be expressed by Eq. (2) [22], [25].

$$J_s = -B\Delta C = -B\left(C_{D,m} - C_{F,m}\right) \qquad Eq.(2)$$

where J_s is the salt flux, B is the salt permeability coefficient and $C_{D,m}$ and $C_{F,m}$ are the concentration value at the membrane active and support layer surface, respectively. The negative sign signifies the opposite direction of salt movement with respect to water.

$$C_{D,m} = C_{D,b}\exp\left(-\frac{J_w}{k}\right) - \frac{B}{J_w}\left(C_{D,m} - C_{F,m}\right)\left[1 - \exp\left(-\frac{J_w}{k}\right)\right] \qquad Eq.(3)$$

$$C_{F,m} = C_{F,b}\exp\left(\frac{J_w S}{D}\right) + \frac{B}{J_w}\left(C_{D,m} - C_{F,m}\right)\left[\exp\left(\frac{J_w S}{D}\right) - 1\right] \qquad Eq.(4)$$

where $C_{D,m}$ is the draw concentration at active layer surface, $C_{D,b}$ is the bulk concentration of draw solution, k is the mass transfer coefficient, $C_{F,m}$ is the feed concentration within the porous support layer, $C_{F,b}$ is the bulk concentration of the feed solution, S is the structural parameter, D is the diffusion coefficient of the salt solution.

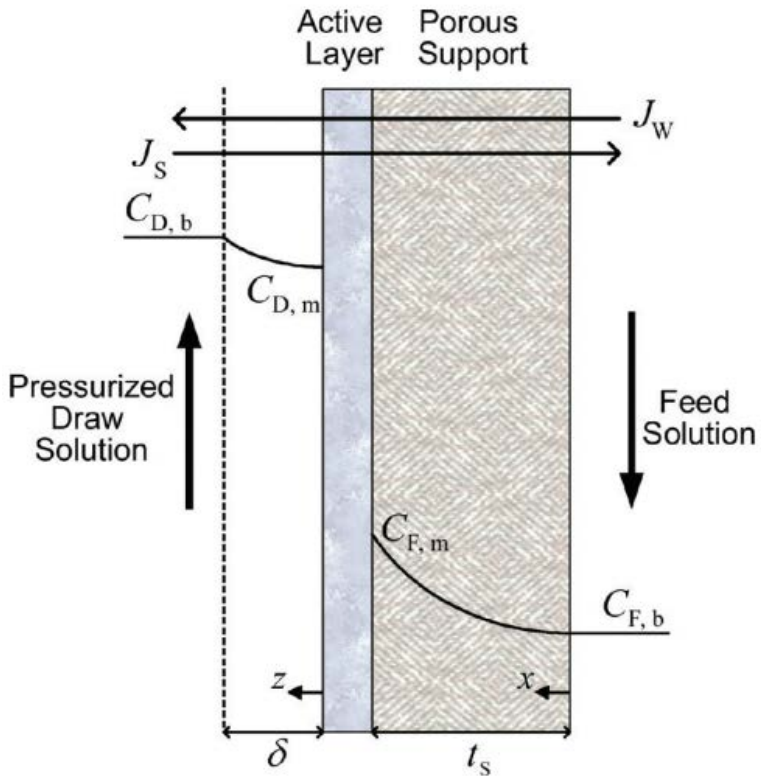

Figure 3: A schematic representation of concentration polarization in a PRO membrane [26]**.** [3]

For the first time, Loeb and Lee et al. [8], [14] observed a steady decrease in the rate of water movement across the PRO membranes, which they termed as "concentration polarization" (CP). As shown in Figure 3, the porous support layer faces the feed solution side, while the active layer faces the draw solution in pressure retarded osmosis. The

[3] Reprinted with permission from "Thin-film composite pressure retarded osmosis membranes for sustainable power generation from salinity gradients" by N. Y. Yip *et al.*, 2011, *Environ. Sci. Technol.*, vol. 45, no. 10, pp. 4360–4369. Copyright © 2011 American Chemical Society.

concentration polarization takes place on both sides of the membrane when water moves across it. CP occurs in two different ways: one is referred to as internal concentration polarization, where the accumulation of salt takes place inside the porous support layer of the membrane, whereas the accumulation of salts outside the membrane active surface is referred to as external concentration polarization. Both internal and external concentration polarization ultimately reduces the effective osmotic pressure difference across the membranes. This results in the movement of reduced water flux across the membrane and thereby reduced power efficiency and a consequent decrease in PRO performance [6], [23], [27].

In 1981, Lee et al. [8] developed the first water flux model to incorporate the effects of concentration polarization in PRO. However, their model only considered the ICP with an assumption of negligible ECP. The expression for their model is described by Eq. (5)

$$J_w = A\left[\pi_{D,m}\frac{1-\frac{C_{F,b}}{C_{D,m}}\exp(J_wK)}{1-\frac{B}{J_w}\,[\exp(J_wK-1)]} - \Delta P\right] \qquad Eq.(5)$$

where, $\pi_{D,m}$ is the osmotic pressure value at the surface of membrane active layer, $C_{F,b}$ is the bulk concentration of the feed, $C_{D,m}$ is the concentration of the draw solution at the surface of membrane active layer, and K is defined as solute resistivity.

In 2009, Achilli et al.[28] modified the Lee et al. [8] model by incorporating the ECP effect.

$$J_w = A\left[\pi_{D,b}\ \exp\left(\frac{-J_w}{k}\right)\frac{1-\frac{\pi_{F,b}}{\pi_{D,b}}\exp(J_wK)\ \exp\left(\frac{J_w}{k}\right)}{1+\frac{B}{J_w}\ (\exp(J_WK)-1)} - \Delta P\right] \qquad Eq.(6)$$

where k is the mass transfer coefficient.

Both, the above models did not take into account the effect of reverse salt flux (RSF). In 2011, Yip et al. [26] modified the Lee model to incorporate the effects of both ECP and RSF in addition to ICP. However, the model assumed osmotic pressure to be linearly dependent on the concentration of the solution using van Hoff Equation. Mathematically, Yip's model is written as,

$$J_w = \left[\frac{\pi_{D,b} \exp\left(-\frac{J_w}{k}\right) - \pi_{F,b}(J_w K)}{1 + \frac{B}{J_w}\left[\exp(J_w K) - \exp\left(-\frac{J_w}{k}\right)\right]} - \Delta P \right] \qquad Eq.(7)$$

$$\Delta\pi = i\Delta CRT \qquad Eq.(8)$$

where i is the van't Hoff's factor, ΔC is the concentration difference, R is the gas constant and T is the temperature

Since then various mathematical models have been developed by modifying the Yip model. Touati et al. [29] developed a model based on the convection-diffusion theory to introduce general mass transfer. Their models take into account all mass transfer of a PRO i.e. its external boundaries, active and a support layer of the real membrane, independently of their effect on the process performance. Mathematically,

$$J_w = A\left[\left(\pi_{D,b} + \frac{B}{A}\left(1 + \frac{A\Delta P}{J_w}\right)\right)\exp\left(-\frac{J_w}{k_D}\right) - \left[\pi_{F,b} + \frac{B}{A}\left(1 + \frac{A\Delta P}{J_w}\right)\right]\exp(J_w K)\exp\left(\frac{J_w}{k_F}\right) - \Delta P\right] \qquad Eq.(9)$$

where k_D and k_F are mass transfer coefficients of the draw and feed, respectively.

iii. Power Density

Power density is an important performance parameter in PRO systems design. As discussed earlier, the minimum power density of 5 W/m^2 of the membrane is necessary for the technology to be commercially viable [30].

Power density is defined as the power output generated per unit area of the membrane in pressure retarded osmosis process. Eq. (10) below shows the mathematical expression of theoretical power density:

$$W = J_w \Delta P = A(\Delta\pi - \Delta P)\Delta P \qquad Eq.(10)$$

where, J_w is the water flux, $\Delta\pi$ is the osmotic pressure gradient and ΔP in the hydraulic pressure gradient.

The maximum power density is obtained on differentiating Eq. (10) with respect to ΔP, which corresponds to a pressure value equal to half of the osmotic pressure difference across the membrane. Mathematically,

$$\mathrm{W_{max}} = A\frac{\Delta\pi^2}{4} \qquad Eq.(11)$$

The value of the osmotic power is directly related to the power density of the membrane. Hence, to generate efficient power using PRO, high power density output is required from the membrane, along with a cheap cost of maintenance and plant operation, as well as capital cost. The power density generated by the osmotic power plant also depends on the feed solution availability and required pretreatment of both feed and draw streams, if any. Thus, the membrane does play a very significant role for efficient power

production. The increased power density may become unprofitable at a point where the cost of production exceeds the output, making the process costly [27].

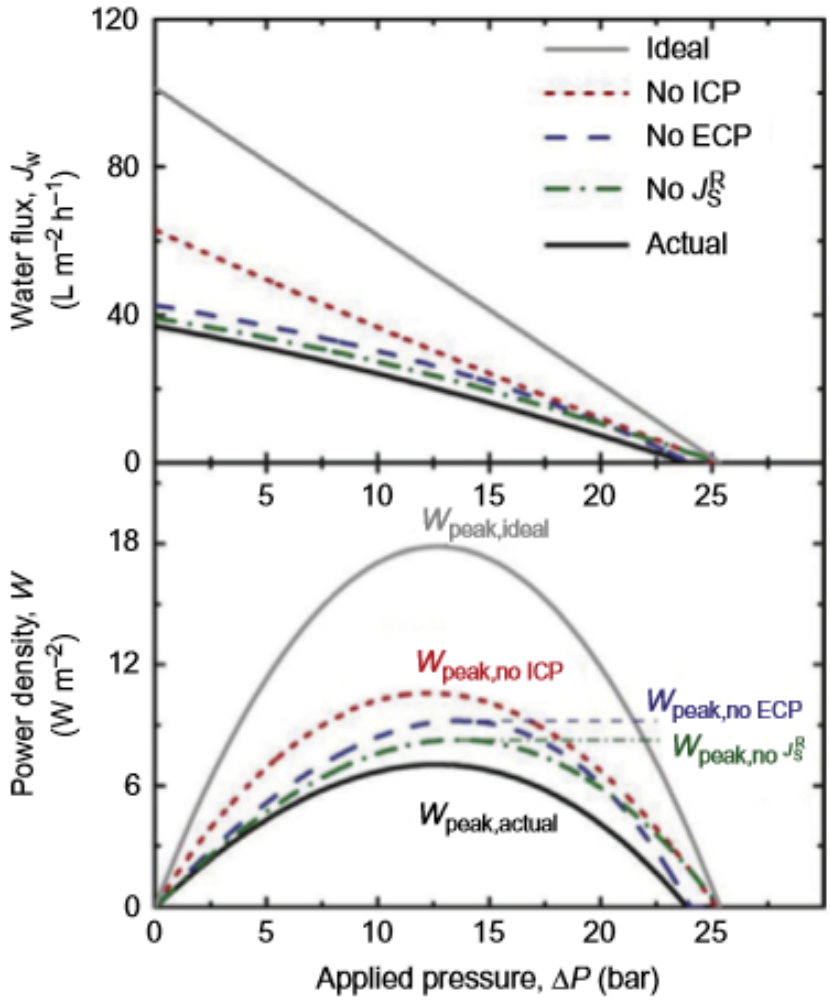

Figure 4: The hydrostatic pressure gradient against the power density and water flux curves for a pressure retarded osmosis process [31]**.** [4]

[4] Reprinted with permission from "Performance limiting effects in power generation from salinity gradients by pressure retarded osmosis" by N. Y. Yip and M. Elimelech, 2011. *Environ. Sci. Technol.*, vol. 45, no. 23, pp. 10273–10282. Copyright © 2011 American Chemical Society.

Figure 4 demonstrates the hydrostatic pressure gradient against the power density and water flux curves for a pressure retarded osmosis process. Similarly, other parameters, i.e., reverse salt diffusion, internal and external concentration polarization, and their effects on the performance of the membrane are also depicted. The water flux linearly decreases with respect to ΔP in an ideal case, resulting in decreased driving force. When the osmotic pressure and applied pressure become equal, the flux value reduces to zero. The power density graph shows an initially increasing and then decreasing trend, as shown in Figure 4. It has been observed that the value of power density and water flux practically decreases due to the combined effect of the reverse salt flux and internal and external concentration polarization. A substantial increase in water flux is observed when internal concentration polarization is neglected. These observations demonstrate that internal concentration polarization is an important factor that reduces the water flux across the PRO membrane [27].

2.3 Membrane and Spacer

The intrinsic transport properties i.e. A, B, and S for the flat sheet membranes are important parameters for simulating the performance of the bench and full-scale PRO processes [32], [33]. Some important parameters need to be taken into account during the operation of PRO membranes. For instance, low flow resistance, low construction cost, high surface to volume ratio, less incorporation of a polarization layer, and high mechanical strength.

Initially, the PRO experiments were conducted using RO membranes. The use of RO membranes led to lower flux, due to the presence of a thick support layer, which led to the

formation of ICP. Recently, efforts have been made to develop PRO-specific membranes [34] or utilize FO membranes. The two classes of membranes currently employed in PRO tests are flat sheet membranes and hollow fiber membranes.

Efficient PRO membranes should have high selectivity, high mechanical strength to withstand high operating pressure and thin support layer to minimize ICP [34]. However, membranes having a thin support layer are limited by mechanical strength to work at higher pressure thus they are supported using spacers which besides providing added mechanical strength also enhances mass transfer [35]. But this added layer of external support also affects intrinsic characteristics of the PRO membranes. Several studies performed in recent years have shown the inadequacy of conventional methods in predicting accurately the A, B, and S for spacer-installed PRO membranes [20], [35]–[39].

2.3.1 Membrane characterization methods

Unlike, the RO and FO membrane characterization where there are set standard protocols, the PRO characterization is still not standardized [40]. On reviewing the literature, the characterization methods for PRO membrane can be classified into three main types:

- Conventional RO-FO method: It consists of two-stage RO and FO experiments for determining the A, B, and S. The values obtained are constant and pressure independent.
- Modified RO method – This method proposed initially by Kim and Elimelech [36] to account for membrane deformation due to high pressure and use of spacers makes use of a modified RO mode performed on a PRO

setup. Since then it has been modified in different studies to give pressure-dependent A, B, and S values.

- Single PRO experiment- The semi-analytical method developed by Kim et al. [38] makes use of a modified FO mode proposed in the earlier study [41] to find variable A, B, and S values based upon the experimental water and salt flux data. In 2016, Lee et al. [39] proposed a statistical approach based upon the single PRO method for calculating constant A, B, and S values.

i. Conventional RO-FO method

FO membranes have been extensively used for PRO studies since the beginning of this century and as such the convention of evaluating the characteristics of FO membranes was also initially adopted for the PRO membranes due to similarity of both the processes. It involves a two-step approach, RO mode of operation is performed to determine the characteristics of the active layer i.e. A and B; the structural parameter of the porous support layer is determined by performing the FO mode of operation [28], [40], [42].

Pure water permeability (A) is determined through the RO experiment, using deionized water as a feed solution. The membrane active layer faces the feed solution. The system is pressurized at different pressure values and water flux is noted, the experimental water flux and the pressure difference is used in Eq. (12) to obtain the value of A with units of liters/meter^2.hour (LMH). Mathematically, it is written as:

$$A = \frac{J_w}{\Delta P} \qquad Eq.(12)$$

where, J_w is the pure water flux and ΔP is the hydraulic pressure difference.

Salt permeability (B) is also determined in RO setup using a 0.1 mM NaCl feed solution with an active layer facing the feed tank and measuring the flux and salt rejection at an operating pressure of 10 bar [42]. Mathematically,

$$B = J_w \left(\frac{1-R}{R}\right) \exp\left(\frac{-J_w}{k}\right) \qquad Eq.(13)$$

where R is the salt rejection and k is the mass transfer coefficient.

The salt rejection is a unitless quantity expressed in terms of percentage and is calculated by measuring the conductivity of the permeate collection tank and feed tank at the end of the RO experiment for determining the B parameter of the membrane [42]. Mathematically,

$$R = \left(1 - \frac{C_p}{C_f}\right) \times 100 \qquad Eq.(14)$$

where, C_p is the concentration of permeate collection tank expressed in terms of conductivity and C_f is the conductivity of the feed tank also expressed in terms of conductivity.

The mass transfer coefficient k in Eq. (13) is determined using the equation given below

$$k = \frac{Sh.\ D}{d_h} \qquad Eq.(15)$$

where Sh is Sherwood number, D is the diffusivity of given salt solution at infinite dilution and d_h is the hydraulic diameter.

The hydraulic diameter is measured in meters and defined mathematically as,

$$d_h = \frac{2(\ flow\ channel\ slot\ width\ \times flow\ channel\ slot\ depth)}{(flow\ channel\ slot\ width + flow\ channel\ slot\ depth)} \qquad Eq.(16)$$

The Sherwood number in Eq. (15) is determined using mathematical relations given below, depending on the nature of flow i.e. whether the flow is laminar or turbulent.

For laminar flow: $$Sh = 1.85\left(Re.Sc\,\frac{d_h}{L}\right) \qquad Eq.(17)$$

For turbulent flow: $$Sh = 0.04(\,Re^{0.75}.Sc^{0.33}) \qquad Eq.(18)$$

where Re is the Reynolds number, Sc is the Schmidt number and L is the length of the flow channel. The Reynolds and Schmidt numbers are calculated using the following formulas:

$$Re = \frac{v.d.\rho}{\eta} = \frac{v.d}{\mu} \qquad Eq.(19)$$

$$Sc = \frac{\mu}{\rho.D} \qquad Eq.(20)$$

where v is the flow velocity, d is the diameter of the flow channel, ρ is the density of the salt solution, η is the dynamic viscosity of the salt solution, μ is the kinematic viscosity of the salt solution, D is the diffusivity of salt solution.

The structural parameter (S) is determined in stage II using the FO experiment, meaning the active layer of the membrane faces the feed solution. The DI water and NaCl solution of 0.5, 1.0, 1.5, 2.0 M are used as feed and draw solutions respectively. The S is determined using osmotic water flux experimentally determined in the FO experiment. Mathematically, it is given as

$$S = \frac{D}{J_w}\ln\left(\frac{B + A\,\pi_D}{B + J_w + A\,\pi_F}\right) \qquad Eq.(21)$$

where, J_w is the osmotic water flux, π_D is the draw solution osmotic pressure and π_F is the feed solution osmotic pressure.

ii. Modified RO method

The conventional two-stage RO-FO experiment process does not give the accurate values of membrane transport properties i.e. A, B, and S for PRO conditions. The values determined using the RO-FO method usually predicts power density values which largely varied from the values obtained by laboraory experiments [43]. The application of high hydraulic pressure in the spacer filled flow channels not only induces physical deformation of the membranes but it also affects the ion transport across the membrane [44], [45], which in turn results in a deviation between the modeled and experimental power density values. The deviation between the two values can be minimized by taking into account the pressure variable A, B, and S values [37].

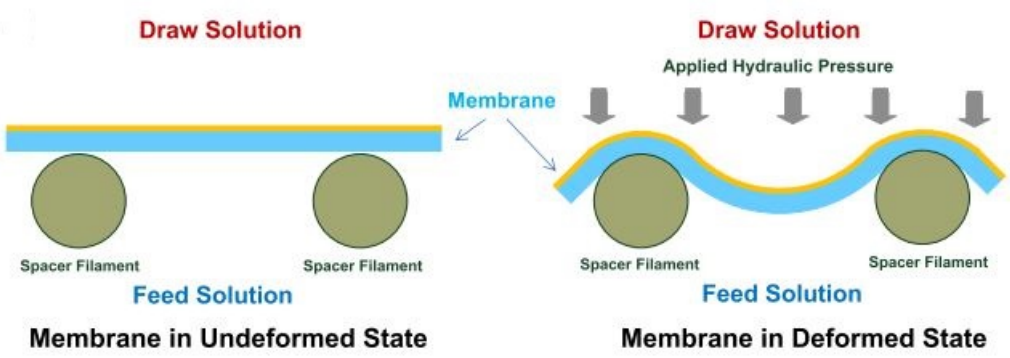

Figure 5: Illustration of membrane deformation due to the use of a spacer [37]**.** [5]

[5] Reprinted with permission from "Effect of feed spacer induced membrane deformation on the performance of pressure retarded osmosis (PRO): Implications for PRO process operation" by Q. She, D. Hou, J. Liu, K. H. Tan, and C. Y. Tang, 2013. *J. Memb. Sci.*, vol. 445, pp. 170–182. Copyright © 2013 Elsevier B.V .

There have been numerous studies done in the past 10 years to incorporate the effect of spacers and high pressure on the intrinsic characteristics of the membrane. The modified RO method [35]–[37] have been extensively tested to experimentally determine the active layer characteristics of the membrane. In the modified RO method first proposed by Kim and Elimelech [36], the PRO setup is operated in RO mode with spacers installed to mimic the PRO specific conditions for better estimation of A and B values. In their study, they used the conventional RO-FO method equations but the estimation of mass transfer coefficient (k) was made by using the correlation put forward by Koutsou et al. [46], where the Sherwood number for spacer filled channel is determined using the Eq. (22) .

$$Sh = 0.2\, Re^{0.57} Sc^{0.4} \qquad Eq.(22)$$

The method was slightly modified by She et al. [37] in their study and put forth a different conclusion i.e the usage of feed spacers with small openings (RO spiral wound permeate carrier) results in better PRO operations at a higher pressure and can negate the effect of membrane deformation which leads to RSF induced ICP in the support layer. Unlike Kim and Elimelech [36], they employed 10 mM NaCl as a feed solution with no circulation of DI water in the permeate channel for determining both the A and B. This was done to study the effect of concentration polarisation while determining A as well and was calculated using Eq. (23) where an extra term in the denominator is to account for the concentration polarisation.

$$A = \frac{J_w}{\Delta P - R\pi_F \exp(\frac{J_w}{k})} \qquad Eq.(23)$$

In 2016, another study was taken up by Hickenbottom et al. [35], they used the modified method similar to Kim and Elimelech [36] in which they not only investigated the effect of different spacer geometries but also their configurations. But the conclusion of their study was similar to that of She et al. [37] i.e. the membrane performance was better on using the spacers with smaller openings such as spiral wound RO permeate carrier.

iii. Single PRO method

Due to the limitations of the above two methods to predict precisely the A, B, and S especially under high pressure, it has become necessary that the intrinsic properties of PRO membranes be determined using a PRO experiment. [38]. In 2015, Kim et al. [38] put forth the concept of apparent solute permeability (B) in pressure retarded osmosis, taking into account the effects of both the osmotic and hydraulic pressure simultaneously for determination of A, B, and S. The equations used for determining A, B and S are the water and salt flux equations developed by Tiraferri et al. for their FO study [41]. The single FO method for determining the A, B, and S was modified to be performed in PRO mode under similar hydrodynamic conditions. It involves a total of four stages as schematically represented in Figure 6, first set of experiments is performed at 15 bar of TMP with 2M NaCl draw against DI feed to obtain water flux and RSF, the experiment is repeated for three more times by diluting the draw solution and recording the water and reverse salt flux for three different draw concentrations. This gives four sets of water and reverse salt flux values which can be used to simultaneously solve Eq. (24) and Eq. (25) to give the values of A, B, and S. The experiment was performed for the remaining 3

stages by using the same membrane but at TMP values lower than 15 bar. Under this method, the salt permeability (B) increased with increasing pressure, pure water permeability (A) decreased slightly with pressure. Also, S was also not affected much by the increase in pressure on the draw side [38], the observation is contradictory to modified RO studies [35]–[37] where S value increased under high pressure.

$$J_w = A\left(\frac{\pi_{D,b}\exp\left(-\frac{J_w}{k_D}\right) - \pi_{F,b}\exp\left(\frac{J_w S}{D}\right)}{1+\frac{B}{J_w}\left[\exp\left(\frac{J_w S}{D}\right) - \exp\left(-\frac{J_w}{k_D}\right)\right]} - \Delta P\right) \qquad Eq.(24)$$

$$J_s = B\left(\frac{C_{D,b}\exp\left(-\frac{J_w}{k_D}\right) - C_{F,b}\exp\left(\frac{J_w S}{D}\right)}{1+\frac{B}{J_w}\left[\exp\left(\frac{J_w S}{D}\right) - \exp\left(-\frac{J_w}{k_D}\right)\right]} P\right) \qquad Eq.(25)$$

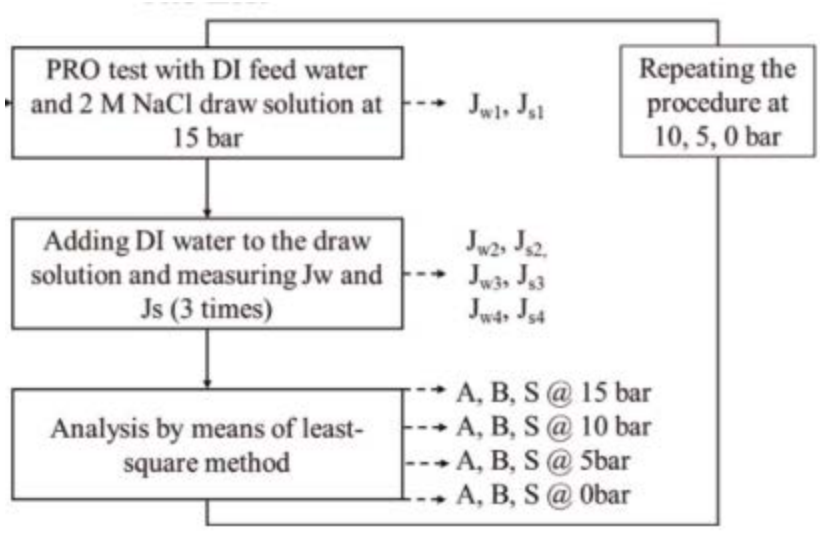

Figure 6: Block diagram of the protocol used in the PRO method for determining A, B and S [38].[6]

In 2016, Lee et al. [39] developed an analytical method for membrane characterization based on a single PRO method, giving constant A, B, and S parameters similar to the conventional method. The work of Lee et al. [39] applies statistical approach based on the existing PRO models [8], [34], [37], [44] to obtain a constant value for transport parameters, with the assumption of no external concentration polarization and constant temperature during the PRO experiment. This allows to compare the values obtained using this method against the values of A, B, and S reported in the literature determined using the conventional RO-FO method. Mathematically,

[6] Reprinted with permission from "Evaluation of apparent membrane performance parameters in pressure retarded osmosis processes under varying draw pressures and with draw solutions containing organics" by J. Kim, B. Kim, D. Inhyuk Kim, and S. Hong, 2015. *J. Memb. Sci.*, vol. 493, pp. 636–644. Copyright © 2015 Elsevier B.V.

$$Minimize \quad f\,(A) = NSTD(B) + NSTD(K_{ICP}) \qquad Eq.(26)$$

where A is the pure water permeability coefficient, $NSTD(B)$ and $NSTD(K_{ICP})$ are the normalized standard deviation of salt permeability and salt resistivity for diffusion within the porous support layer, respectively.

The math model of Lee et al. [39] is defined for an optimization problem and is solved on an excel spreadsheet by employing an evolutionary algorithm. In their optimization model, they normalized the standard deviation value of salt permeability coefficient (B) and feed solution salt resistivity for diffusion (K_{ICP}) by dividing by their respective mean values, the normalized value is based on experimental data from reference literature. The K_{ICP} for different pressure values of the experiment as mentioned in reference literature [37] is determined by using salt flux and concentrations values of feed solution at various locations i.e. of bulk fluid, support layer surface, and within the porous support structure. The concentration value of feed solution at the support layer surface and inside the porous support structure is determined based on the water and solute characteristic value along with the hydrodynamic condition in the feed flow channel.

2.3.2 Feed spacer design and its impact

As seen in the previous section the usage of spacers increases the solute permeability (B) characteristic of the membrane especially at higher pressure but it is necessary to prevent membrane rupturing. In a PRO assembly employing the flat sheet membrane modules, spacers are used on the feed as well as draw side flow channels. The feed spacer design is critical to PRO performance, it is used for (1) maintaining the structural integrity of flow channel, (2) promote better diffusion across membrane surface by enhanced

turbulence, and (3) mechanically support the membrane under high pressure. Thus, the spacers in PRO serve the dual purpose of both the spacer as well as permeate carriers [37]. The traditional feed side spacers used in PRO have fairly large openings compared to permeate carriers used in the RO which leads to membrane deformation under high pressure [36], [47], [48]. The deformation of the membrane leads to performance reduction of the PRO due to (1) increase in the reverse salt diffusion, which leads to enhanced ICP [48], (2) increased value of salt permeability coefficient [36], and (3) increased hydraulic pressure loss on the feed channel side [36], [48].

The design of spacers with an improved flow channel can help to overcome the above-mentioned challenges of reduced mass transfer and energy loss. The experimental study was done by Kim et al. [36] and She et al. [37] make use of three different spacer samples for studying the impact of spacer design on the system performance . It was observed on using the spacers that the membrane develops convex and concave imprints on the support and active layer respectively. This suggests the structural deformation is permanent and is not reversed on reducing the trans-membrane pressure. In their study, Kim and Elimelech [36] also put forward the concept of shadow effect which can obstruct the permeate flow rate in PRO. At high hydraulic pressure the membrane strands are pushed against the spacer surface, this, in turn, reduces the available area for water permeation.

The spacers are characterized by using a number of channels per inch, its thickness, filament diameter in mm, opening size in mm (distance between adjacent filaments), and opening ratio or voidage which represents the opening area in the spacer.

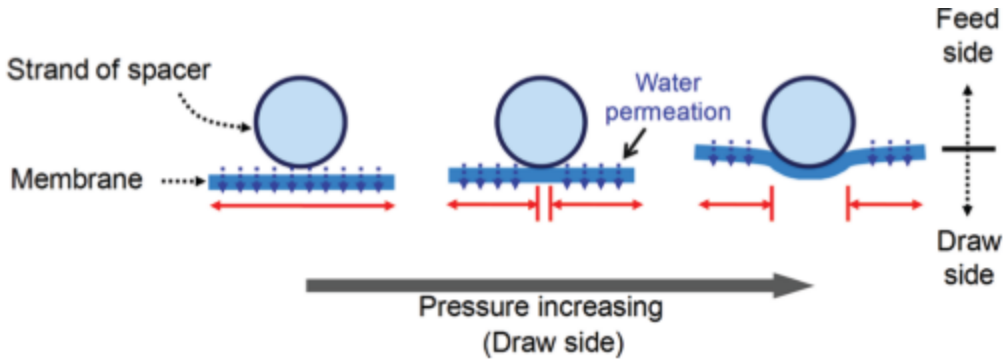

Figure 7: Schematic representation of the Shadow effect on the membrane [36].[7]

2.4 Draw Solutions

2.4.1 Brines

The rapid development of the PRO as detailed in section 2.2 of this study was motivated by the availability of natural and synthetic high salinity brines. In recent decades the focus for wastewater and brine management has shifted from 'treatment and discharge' to 'recycle and resource recovery'. Broadly, the sources of hypersaline water can be classified as natural brines and industrial brine [22].

i. Natural brines

The natural sources of high salinity solutions are present in the form of hypersaline lakes, salt domes, and geothermal water. The lakes with salinity ranging from 5 wt. % to 44 wt. % are present in nature [27]. The feasibility of using the Dead Sea and Great Salt

[7] Reprinted with permission from "Adverse impact of feed channel spacers on the performance of pressure retarded osmosis" by Y. C. Kim and M. Elimelech, 2012. *Environ. Sci. Technol.*, vol. 46, no. 8, pp. 4673–4681. Copyright © 2012 American Chemical Society.

Lakes was reported by Sidney Loeb [17], [18]. Kelada in his report listed the hypersaline lakes across different continents [49]. Some of these lakes were evaluated and recommendation for feed water was made depending on the geographical location of the hypersaline lakes which are typically endorheic lakes, meaning lakes which lack an outflow. Although, hypersaline lakes are a rich source of energy their remote locations make them unattractive due to higher cost for transmission of produced power [22].

Salt domes are salt deposits found underground; due to the lower density of the salt layer compared to the surrounding geological layers it moves up towards the surface forming a dome structure. Wick and Isaacs [50] for the first time proposed the idea of hypersaline draw solutions from salt domes. Sea or river water is pumped to the salt dome to produce brine which is then interfaced with less saline feed to produce energy. The dilute mixture can then be disposed into the sea. They predicted a single salt dome of 1 km^3 holds the capability to produce 77 TWh energy for a combination of saturated brine and seawater [51]. In their study, they listed the salt domes with bigger sizes ranging up to 40 km^3 meaning the potential of energy production using underground salt domes in PRO is huge. However, a drawback associated with the use of salt domes based PRO scheme is the environmental impact due to discharge of brines in the sea, which can be mitigated by discharging the brine into streams flowing to the brine lakes or discharge to seawater flowing into coastal salt pans [52]. Secondly, instead of producing the brine from salt domes, PRO can utilize the brines already generated from other activities around the salt domes [22].

Hypersaline geothermal water is another potential source for PRO. In many parts of the world, this heated underground water found at depth of 1-2 km from the surface is already used in district heating. Recently, the initiative by SaltPower, a Danish company, for utilization of geothermal water for both heating and electricity generation intended to lower the capital cost for power production using PRO has been suggested. Similar to salt domes, the major issue of this PRO scheme is also the brine disposal [22].

ii. Industrial Brines

Industrial brines are those that are produced by various industries such as desalination plants, food processing, leather industry, and chemical and petroleum industry. In 2013, worldwide RO plants with an estimated recovery of 40 % produced about 31,000,000 m^3/day of desalination brines having a salinity of 1.07 M of NaCl [22]. These plants are generally located near to municipal wastewater treatment plants such as Mega-ton Water System built in Japan, which has low salinity and can be utilized as feed streams to the PRO process. For a PRO plant scheme, with desalination brine and municipal wastewater as draw and feed, respectively, global power production of 365 MW was estimated by Madsen et al. [53] having typical 40% efficiency used for evaluating seawater based PRO. The drawback of using such a scheme is the occurrence of severe fouling on the feed side, which can be mitigated depending on the level of pre-treatment. The results obtained from the Mega-ton Water System pilot study show using UF-LPRO for feed treatment can reduce the fouling thereby giving stable energy production for a year [54].

Fracking wastewater or Produced water, is the waste stream produced during the extraction of oil and gas. The salinity of produced water varies from location to location

but is usually characterized by high salinity. The Permian basin generated produced water with TDS concentrations ranging from 0.5 to 40 wt% [55]. Similarly, Thiel et al. in his studies on the treatment of produced water reported the high average wt% from three locations, for Nova Scotia 5.9 wt%, for Marcellus Shale 14.5 wt%, and for Permian Basin 18.3 wt% [56], [57]. In addition to concentration, salt composition is equally important with the major ions being sodium, calcium, magnesium, potassium, chloride, sulfate and bicarbonate. Sodium is the major cation while the Chloride is the major anion in the water produced from the conventional wells. Also, the dominant salt type is an important descriptive factor reflecting the formation environment around the well; the sodium chloride is the dominant salt present in produced waters from conventional wells [58]. The Management of produced water is limited to its use for enhanced oil recovery (EOR), deep well disposal, or disposal into evaporation ponds [59]. The large quantity of hypersaline produced water offers an opportunity to utilize it as draw stream for power production in PRO technology.

In addition to desalination brine and produced water, there are other industries such as food processing, wine, leather, and chemical which generate large quantities of brines. Some of them such as the dairy industry has been reported in the literature to produce waste brine as high as 23.5 wt% from cheese production [60]. Similarly, the brines produced in vegetable, leather coal, and chemical industries have been reported to be more than two times of seawater salinity with a combined volume of several million tons generated per year [61]–[64]. These wastewaters though having high salinity are difficult

to use in PRO, mainly because of their varying quality which may necessitate pre-treatment and prevent the use of standard design for their application.

2.4.2 Characteristics of brine solutions

The use of hypersaline solutions in the PRO is governed by certain characteristics that can serve as a screening criterion to determine the efficiency of using such solutions. As discussed earlier there are several PRO schemes based on a combination of the draw and feed solution, the use of hypersaline solutions mentioned in the previous section might not be efficient for one scheme but can work for the other scheme. Two of the major characteristics are (1) Gibbs energy of mixing which determines the maximum energy thermodynamically possible and (2) osmotic pressure difference which determines the magnitude of driving force. These can be determined analytically using the equations found in the literature [30], [65]. For synthetic solutions, the solubility, diffusivity, and hydration radius of the solutes can also be evaluated to produce PRO specific hypersaline solutions. The synthetic solutions are further classified in the literature as organic and inorganic depending on the type of salt being used [66], [67].

i. Gibb's Free Energy of Mixing

For understanding whether the salinity gradient energy (SGE) is viable or not, it is necessary to determine the maximum theoretical energy available due to the mixing of the solutions. The maximum available energy from the reversible PRO process is equal to the Gibbs free energy of mixing, ΔG [68]. This provides the maximum energy possible for a system working under ideal condition, the value is always less for a real system. The maximum Gibbs energy for a given pair of draw and feed solution can be determined

analytically using Eq. (27). The maximum energy is dependent upon the initial concentration of the feed and draw solutions, where the typical optimal feed fraction (∅) to reach maximum free energy of mixing is 0.6 i.e. 60 % of the source water is taken from feed and remaining 40% is taken from the draw tank [69].

$$\Delta G_{max} = \left[\frac{c_{D,b} c_{F,b}}{c_{D.b} - c_{F,b}} \left(\ln\left(c_{D,b}\right) - \ln\left(c_{F,b}\right) \right) - \exp\left(\frac{c_{D,b} \ln\left(c_{D,b}\right) - c_{F,b} \ln\left(c_{F,b}\right)}{c_{D,b} - c_{F,b}} - 1 \right) \right] \times iRT \qquad Eq.(27)$$

where, $c_{D,b}$ and $c_{F,b}$ are the initial bulk concentration of the draw and feed respectively, i is the van't Hoff factor, R is the universal gas constant and T is the temperature.

ii. Osmotic Pressure

As an alternative to the free energy of mixing, osmotic force is the important parameter to determine the suitability of the solution for the given PRO scheme. The osmotic gradient is the driving force in PRO and it is necessary to accurately determine the same. For ideal and low molarity solutions, the traditional van't Hoff equation Eq. (8) provides reasonable estimates.

However, for hypersaline solutions, van't Hoff's equation becomes highly inaccurate and a rigorous Equation of State (EoS) would be required for accurate estimates of osmotic pressure. Also, osmotic pressure can be obtained experimentally by measuring the water activity (a_w) and applying the following equation [70],

$$\pi = \frac{-RT}{v_{H2O}} \ln a_{H2O} \qquad Eq.(28)$$

where, v_{H2O} is the molar volume of the water and a_{H2O} is the activity of water in the solution. The value for molar volume and the activity can be determined theoretically using methods such as Pitzer equations or for NaCl solutions that can be obtained from the literature [71]. The OLI Systems, Inc. (Morris Plains, NJ), a commercial tool used for calculating the osmotic pressure is also based upon the activity model.

Wilson and Stewart proposed an alternative empirical equation for predicting osmotic pressure which is pretty similar to van't Hoff's equation but uses molality (mol/kg of solvent) instead of molarity,

$$\pi = i\rho bRT \qquad Eq.(29)$$

where ρ is the density of the solution, b is the molality.

The use of molality has benefit as it is independent of density, still, Eq. (29) is not very precise as it doesn't account for the solute-solvent interaction. In order to overcome this shortcoming, Wilson and Stewart introduced a "bound water" term in their model [70]. Bound water terms account for the water molecules which bind with cations and become part of the solute instead of solvent. Using, the theory of modified molality, Wilson and Stewart produced a better estimate of the osmotic pressure values. Mathematically it is written as,

$$\pi = i\rho\left(\frac{n_s}{m_w - h.n_s.MW_w}\right)RT \qquad Eq.(30)$$

where, n_s is the number of moles of solute, m_w is the mass of the water, h is total waters of hydration per mole of solute and MW_w is the molecular weight of water.

Bajraktari et al. [22] presented a simplified linear equation for calculating osmotic pressure in hypersaline solutions containing majorly NaCl. These equations were obtained

after regression fitting of the activity model with each having a regression coefficient value of more than 0.999. The fitted equations for different concentration units are presented in Table (1) below.

Table 1: Fitted equations for osmotic pressure based on activity model [22].[8]

Unit of concentration	The fitted equation for osmotic pressure
Weight percent (wt/wt %)	$\pi = 0.00995c^3 + 0.02553c^2 + 8.197c - 0.766$
Molarity (mol/litre)	$\pi = 0.6311c^3 + 2.636c^2 + 44.85c - 0.09478$
Molality (mol/kg solvent)	$\pi = 0.1921c^3 + 2.911c^2 + 43.44c - 0.4509$
Mass concentration (g/L)	$\pi = 3.16210^{-6}c^3 + 7.71710^{-4}c^2 + 0.7674c - 0.09478$

Manzoor et al. in their study determined the osmotic pressure for electrolytic solutions using Equation of state (EoS) [21]. The EoS developed by them is derived based on Helmholtz energy, which allows determination of thermodynamic properties by changing Helmholtz energy into the fugacity coefficient. The advantage of their EoS is the easily measurable input parameters i.e. temperature, pressure, and composition of the solution for the determination of molar volume and osmotic pressure as follows,

$$x_s^I \varphi^I_{s,(T_s,P_s^I,x_s^I)} P_s^I = x_s^{II} \varphi^{II}_{s,(T_s,P_s^{II},x_s^{II})} P_s^{II} \qquad Eq.(31)$$

[8] Reprinted with permission from "Pressure retarded osmosis from hypersaline sources — A review" by N. Bajraktari, C. Hélix-Nielsen, and H. T. Madsen, 2017. *Desalination*, vol. 413, pp. 65–85. Copyright © 2017 Elsevier B.V.

where, x_s^I and x_s^{II} are the mole fraction of the solvent in the solution and in the pure solven,t; φ_s^I and φ_s^{II} are the fugacity coefficients of the solvent in the solution and pure solvent, P_s^I and P_s^{II} are the pressure of the solvent in the solution and pure solvent respectively. The pressure of the pure solvent is chosen to be 1.01325 bar and Eq. (31) is then solved for P_s^I by satisfying the equilibrium condition. The osmotic pressure of the solution is then obtained by using the relation given below

$$\pi = P_s^I - P_s^{II} \qquad Eq.(32)$$

iii. Diffusion Coefficient

Diffusion is defined as a movement of constituent particles relative to bulk fluid motion due to concentration differences within a solution. The diffusion coefficient (D) is used to represent the phenomenon of diffusion, it corresponds to the solution i.e. it is the same for both the solute and the solvent. In PRO, the diffusion coefficient of the solution is necessary for estimating the transport properties of the membrane and also to study the effect of using different solutions to overcome the concentration polarization problem. It has been observed if the salt has higher diffusivity it readily diffuses from an area of high to low concentration and reduces the effect of dilutive ECP at the active layer surface [67]. Mathematically, the diffusion coefficient at infinite dilution for the individual ions and the binary electrolyte is given by using the Nernst-Einstein equation [72].

For ions: $$D_i = \frac{R.T.\lambda_i}{|z_i|.F^2} \qquad Eq.(33)$$

where, D_i is the diffusion coefficient of the species i, R is the universal gas constant, λ_i is the ionic equivalent conductance, z_i is the charge number of species i and F is the Faraday's constant

For electrolyte $$D = \frac{D_+ D_-.(z_+ - z_-)}{z_+.D_+ - z_-.D_-} \qquad Eq.(34)$$

where D is the diffusion coefficient of the electrolyte.

3. METHODOLOGY

This chapter describes in detail the construction of the PRO setup and methods employed to perform experiments. Firstly, the intrinsic properties of membranes were characterized using the conventional RO-FO method. The PRO experiments were performed to measure the water flux and corresponding power density at various pressures. Simultaneously, the osmotic pressure for draw solutions used in PRO experiments is also determined experimentally.

3.1 Assembly of PRO setup

The materials used for the PRO setup assembly were designed and manufactured to be compatible with high pressure and salinity conditions. PRO experiments were performed using the SEPA cell system produced by Sterlitech (USA). The SEPA cell system has a convenient hydraulic clamping holder, it makes use of hydraulic-powered piston to hold the cell plates together. The cell plates are made up of 316SS material which prevents corrosion on using high salinity solution and each of these plates has identical flow channels with the only difference being the presence of a 1.9 mm deep allowance in the bottom plate. This allowance in the bottom plate is designed to house the spacer and membrane support plate. The spacers are used on both sides of the membrane in the PRO experiment whereas the support plate is only used on the feed side. Three types of the spacer were used in this study, two of them are the standard net type with extruded mesh commercially available from Sterlitech and the third one is tricot RO permeate carrier obtained from an RO spiral membrane module available in the lab. The spacers were characterized based on a number of openings per inch and their thickness. The one-piece

of extruded mesh spacer with diamond shape openings is only used on the draw side whereas the net and tricot spacer with smaller openings are installed on the feed side. Properties of the spacers are mentioned in Table 2 below.

Table 2: Properties of the spacers

Spacer type	Thickness (mm)	Opening size (mm)
Extruded Diamond shape	0.65	2.50
Extruded net type	0.20	< 1.00
Tricot net type	0.20	< 0.50

The membrane is supported further on the feed side using the support plate. Two different designs of the support plate were used in the study. The first one is a standard SS316 grade obtained from Sterlitech. The second one is 3D printed internally in one of the university labs using Ultimaker tough PLA material with straight flow channels along the length of the plate. This second plate was designed in a way so as to prevent the spacer from sticking to the surface under high pressure which results in pressure build-up on the feed side.

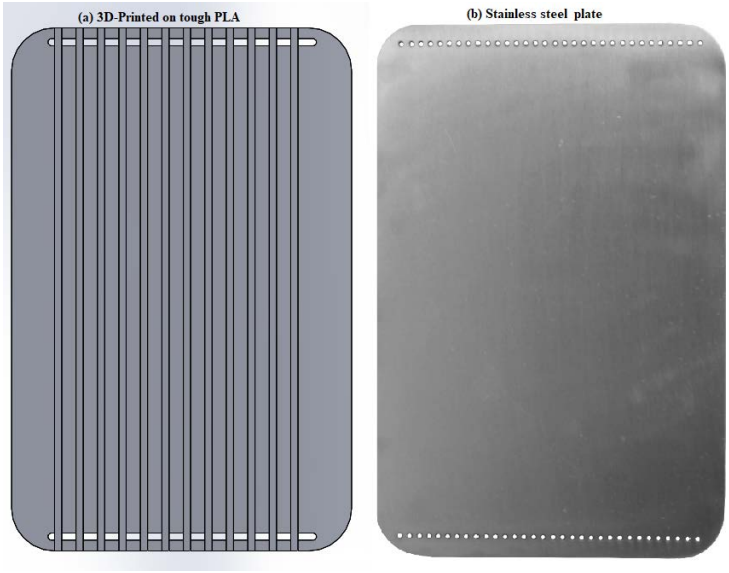

Figure 8: Membrane support plates (a) 3D printed support plate on tough PLA material (b) Sterlitech 316SS support plate

Other key components of the PRO unit were the pumps on the draw and feed side of the PRO setup from Wanner Engineering and Cole Parmer, respectively. The five liters plastic containers were installed for storing the draw and feed solutions which were placed on top of weighing scales (AND FZ-5000i) and the concentration change of the solutions was determined using conductivity probe (Sensorex EX2000RS). The temperature (Omega PR-21) and pressure transducers (Omega PXM409) along with the flowmeters (Atrato, Ultrasonic) were connected along the connection pipelines to record the real-time physical properties of flowing streams. The assembled module was further connected to the Swagelok back pressure regulator on the draw flow line, used for exerting the pressure on the draw solution inside the cell plate. For safety, the pressure relief valves were installed on the draw and feed connection channels which prevent the high pressure build-

up. The entire setup was housed on the nylon structure manufactured in the university machine shop.

The sensors in the PRO assembly were connected to the data acquisition system (DAQ). The DAQ system controller was programmed on a computer using LabVIEW software to record the values from the sensors into an excel file, which can be retrieved at the end of the experiment for processing the data.

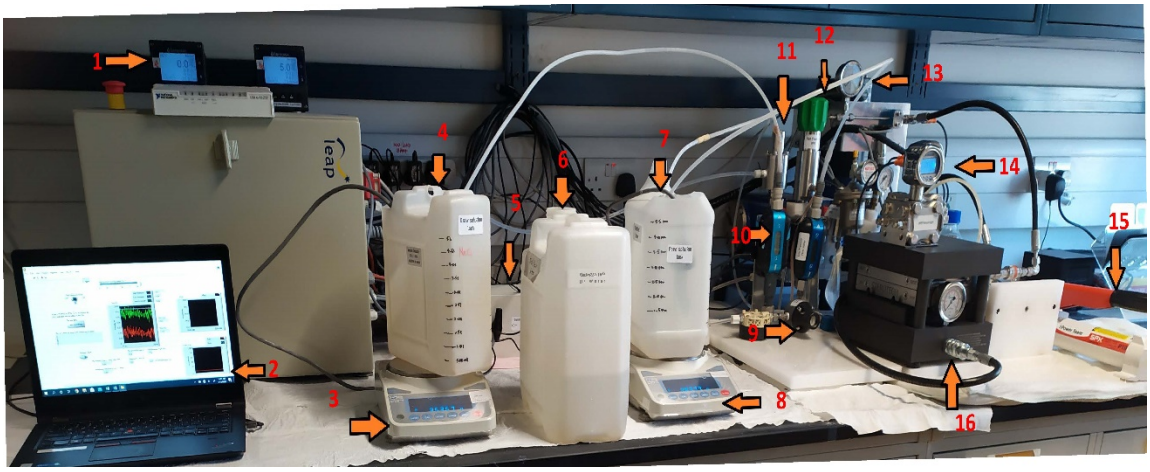

Figure 9: PRO experimental setup. From left to right. (1) The conductivity meters, (2) The computer with LabVIEW interface window, (3) The draw tank weighing scale, (4)Draw solution tank, (5) Supply lines regulator box, (6) DI water tank, (7) Feed solution tank, (8) The feed tank weighing scale, (9) LP relief valve, (10) Flow meters, (11) HP relief valve, (12) Back pressure regulator, (13) HP gauge, (14) Pressure differentials, (15) Hydraulic hand pump, (16) SEPA membrane unit.

3.2 Experimental Design

3.2.1 Solutions and membranes

Honeywell ACS-grade salts were used for preparing the salt solutions. The Deionized water (DI) was obtained from the MilliQ water system in the lab. The concentration of solutions was based on molarity i.e. moles of salt per liter of solution. The required mass of salt was measured on a scale and put in a volumetric flask. The solution was prepared in a flask by pouring water till halfway mark and stirred, once the salt dissolves additional water was poured till the level reaches 1-litre mark. The different molarity solutions were prepared in advance and stored in different five-liter containers to be used later to recharge the solution tanks when needed. The conductivity of these freshly prepared solutions was also measured and recorded.

The FTS cellulose tri-acetate (CTA) and Toray thin film composite (TFC) flat sheet commercial membranes were used in this study. The membranes coupons were cut to fit the size of the cell using a steel die. They were covered with a water-resistant tape along the edges in order to prevent rupture and damage to the membrane at high pressures [20]. The membranes were stored as recommended by the manufacturer in a moist and cold environment inside plastic containers. Before initiating the experiment, the virgin membranes were compacted at the maximum hydraulic pressure value intended to be used during PRO operation i.e. 60 bar in this study by circulating deionized water (DI) for a minimum of 10 hours [20]. This allowed permeate transfer across the membrane to become steady. One can also leave the membrane for compaction overnight if the

experiments are to be performed the next day. Water flux across the membrane was determined using Eq. (33)

$$J_w = \frac{\Delta m}{t.A_m} \qquad Eq.(33)$$

where Δm is the mass change in the feed supply tank, t is the time of experiment and A_m is the available membrane area for the mass transfer to occur.

3.2.2 Experimental determination of membrane intrinsic properties

In this study, the conventional method as discussed in section 2.3.1 was employed for determining the intrinsic characteristics of the membrane. Pure water permeability (A), salt permeability (B), and structural parameter (S) of FTSH2O and Toray membranes were determined using a series of RO-FO experiments. For RO experiments the Sterlitech CF042D assembly is used and FO experiments are performed on CF042A assembly.

The A and B characteristics were determined during stage I using the CF042D RO unit. In order to determine A, the compacted membrane was placed inside the CF042D cell assembly such that the active layer was facing the feed tank containing the DI water. The cross-flow velocity was set at 0.25 m/s and the bar maximum transmembrane pressure (TMP) at which the experiment performed was 10 bar [42]. The flux values and corresponding A values calculated using Eq. (33) and Eq. (12) were recorded for three different TMPs. The slope of pure water flux over applied pressure was used to determine the value of the A parameter. Similarly, for calculating B, the DI water is replaced with 0.1 mM NaCl solution while transmembrane pressure and cross-flow velocity were fixed at 10 bar and 0.25 m/s, respectively, with the active layer of the membrane facing the feed

tank containing the NaCl solution [42]. The water flux across the membrane from Eq. (33) and salt rejection rate using Eq. (14) are recorded every two hours and the total experiment time is six hours and upward. Eq. (12) was used to determine B and the mass transfer coefficient (k) was determined using Eq. (15).

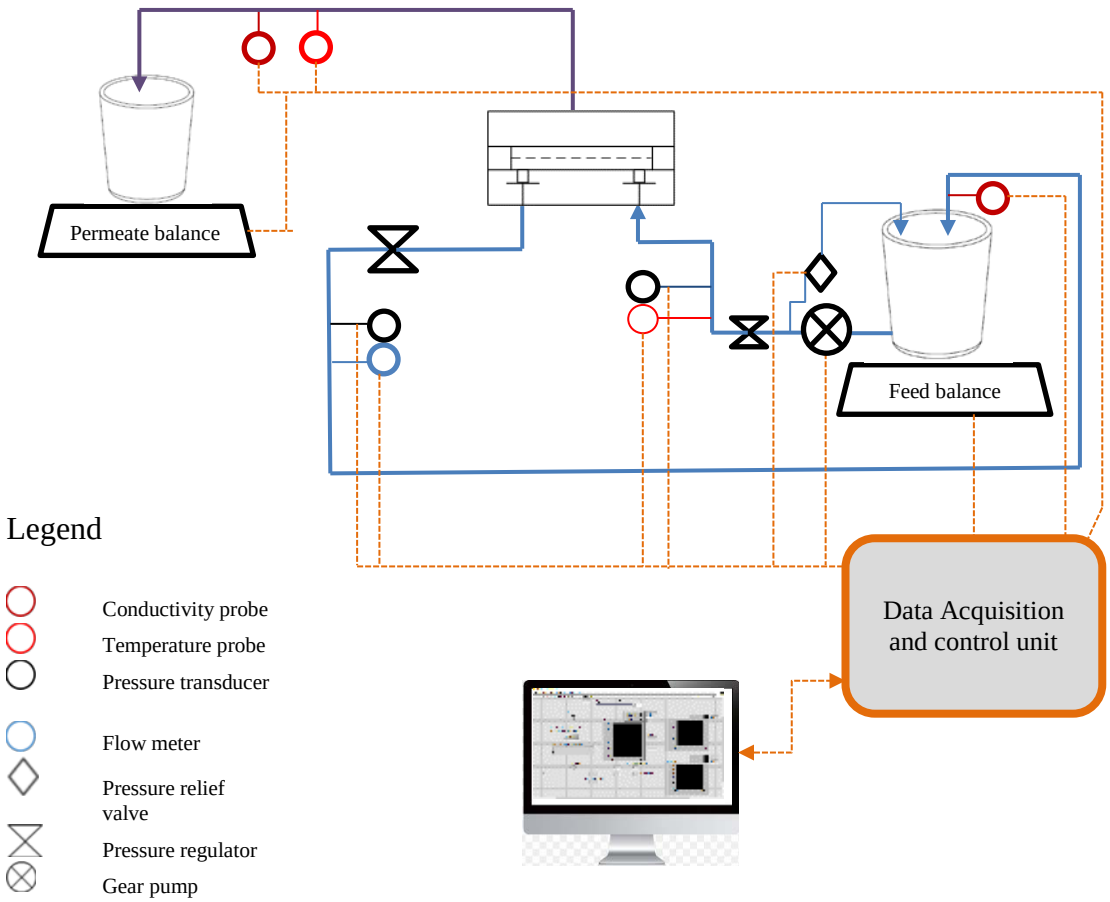

Figure 10: Process flow diagram of RO setup.

The FO mode of operation was used for determining the structural parameter (S). The CF042A assembly was used to measure the osmotic flux using the deionized water (DI) as the feed solution and the NaCl solution of 0.5 M concentration as the draw solution. In FO mode the active layer of the membrane was oriented towards the feed solution and the support layer faces the draw solution. Transmembrane pressure was almost negligible, with no pressure being applied on either side inside of the cell, osmotic pressure acts as a driving force. The experiment was conducted with a cross-flow velocity of 0.014 m/s [42]. Osmotic flux was calculated by recording the change in mass on the feed tank due to water permeating from the feed to the draw side over a fixed time interval. To obtain the numerical value of the structural parameter (S), Eq. (21) was used by substituting the values of A and B obtained from stage I.

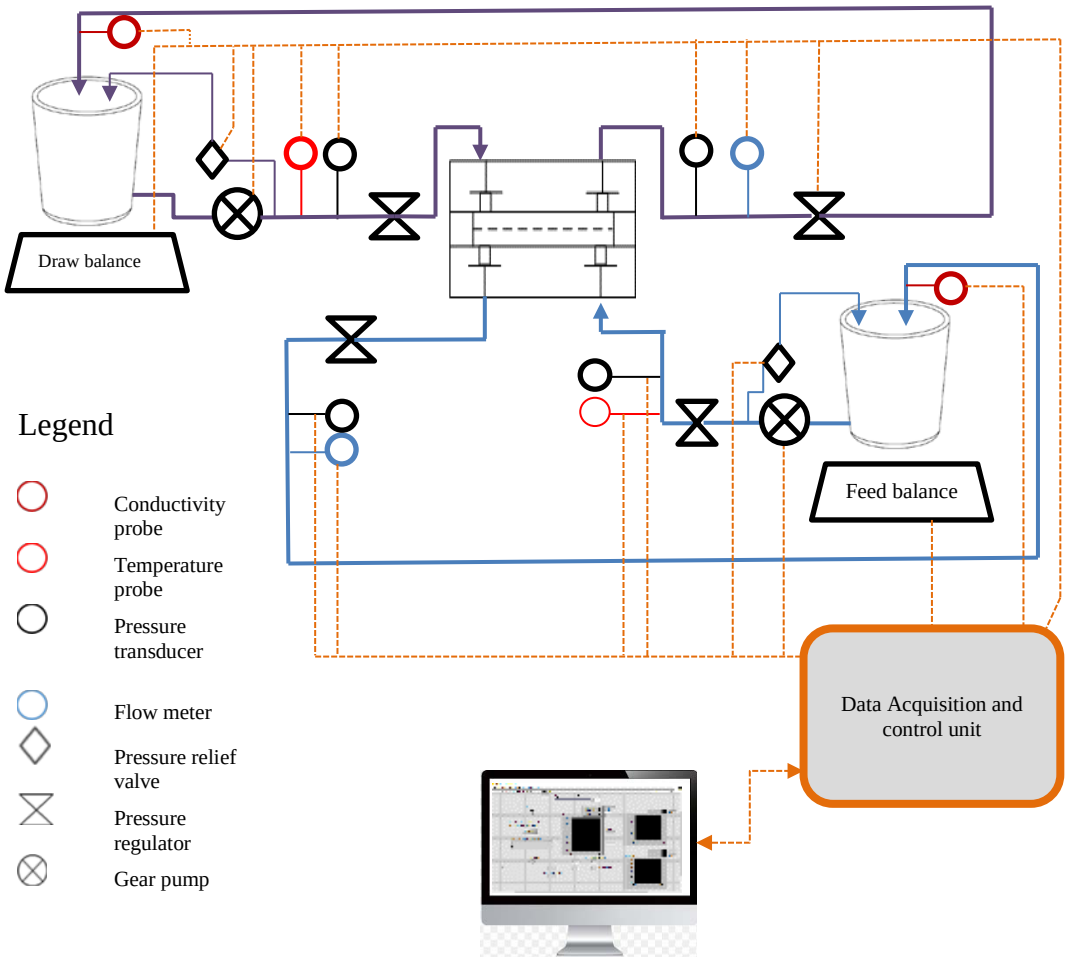

Figure 11: Process flow diagram of FO setup.

3.2.3 Pressure Retarded Osmosis (PRO) Experiment

The PRO experiments were conducted to measure the water flux across the flat sheet membranes and use it to calculate corresponding power density at different transmembrane pressures. Before placing the compacted coupon of the membrane inside

the cell, it was rinsed with DI water to remove traces of preservative or solid particles from its surface. The membrane was then placed inside the cell with the active layer facing the draw side. Also, the spacers and support plate was installed, as mentioned in section 3.1 of this report.

Once the membrane was installed and the cell plates were clamped properly, the PRO experiment was initiated by recharging the draw and the feed tank with the required solution. In the PRO experiment, 4 liters of NaCl salt solutions ranging from 0.6 M to 3 M were used as draw solutions, while the feed tank was loaded with 4 liters of DI water or different concentrations of NaCl solution such that its molarity is always less than the draw solution. The experiment started by turning on the pumps and adjusting the flow rate to 40 ml/min by varying the pump speed. Then, the hydraulic pressure was increased gradually on the draw side using the back pressure regulator (BPR). This resulted in transmembrane pressure (TMP) being developed across the membrane. The TMP was formed due to both the flow of the solution and the closing of the BPR. After the desired TMP was achieved and the flow rate was fixed, the system was allowed to stabilize for 10 minutes, such that water starts permeating from the feed to the draw side. At the same time the salt concentration in both tanks was monitored using the conductivity probe and were checked against the recorded values of a fresh sample of different salt solution. Conductivity values of different NaCl solutions are also cross-checked with values obtained from OLI software, and the two values were found to be in agreement with a deviation within ±5 mS/cm. The membrane burst pressure was determined by observing the feed tank conductivity value, membrane active layer was considered to be damaged if

the conductivity value of the feed tank increased by more than 1500 µS/cm over 10 minute time period [35]. Additionally, on rupturing of the membrane there was a sudden pressure drop on the draw side.

Once the experimental conditions were ensured to be at the required settings, the PRO data was recorded using the LabVIEW interface for different time intervals, it automatically records the data from flow meters, pressure sensors, temperature and conductivity probes and weighing scale in an excel file. The data extracted from LabVIEW were used to calculate the final water flux using the Eq. (33). This flux value was then placed in Eq. (10) to calculate the power density at the particular TMP.

Before performing the experiment for the new pressure value, the system was washed with DI water. To do that, the supply on the feed and draw side inside the cell plates were changed to 10 liters DI water tank using gate valves, and a depressurized wash cycle is performed by circulating DI water at high flow rate on the draw and the feed side for around 5 minutes. This was done to clean residual salt particles from the flow lines, spacers, membrane and space between cell plates. It also helps to prevent corrosion of the pipelines and flow channels. Second backwashing was performed at a low flow rate where the feed side was pressurized and draw side was kept at atmospheric pressure, this caused the flow of water molecules across the active layer into the support layer thereby removing the deposit of salt particles. The salt solutions were reused for the next pressure run by dosing with stocked saturated NaCl solution and measuring the conductivity using the probe, to ensure the desired concentration is restored before starting the experiment. After

running the experiments for complete pressure range using a particular feed and draw solution combination as detailed above; the membranes, spacers, and cell plates were removed from the holder and cleansed physically by rinsing with DI water.

The flux and power density values obtained for different pressure runs were used to determine the feasibility of the particular membrane for power generation under the stated conditions i.e. feed and draw solution combination, flow rate, temperature, pressure, and spacers configuration. Based on the values obtained for different conditions the setup was re-configured to perform the final experiment under most favorable conditions using the CTA membrane along with 3D printed support plate and tricot spacers.

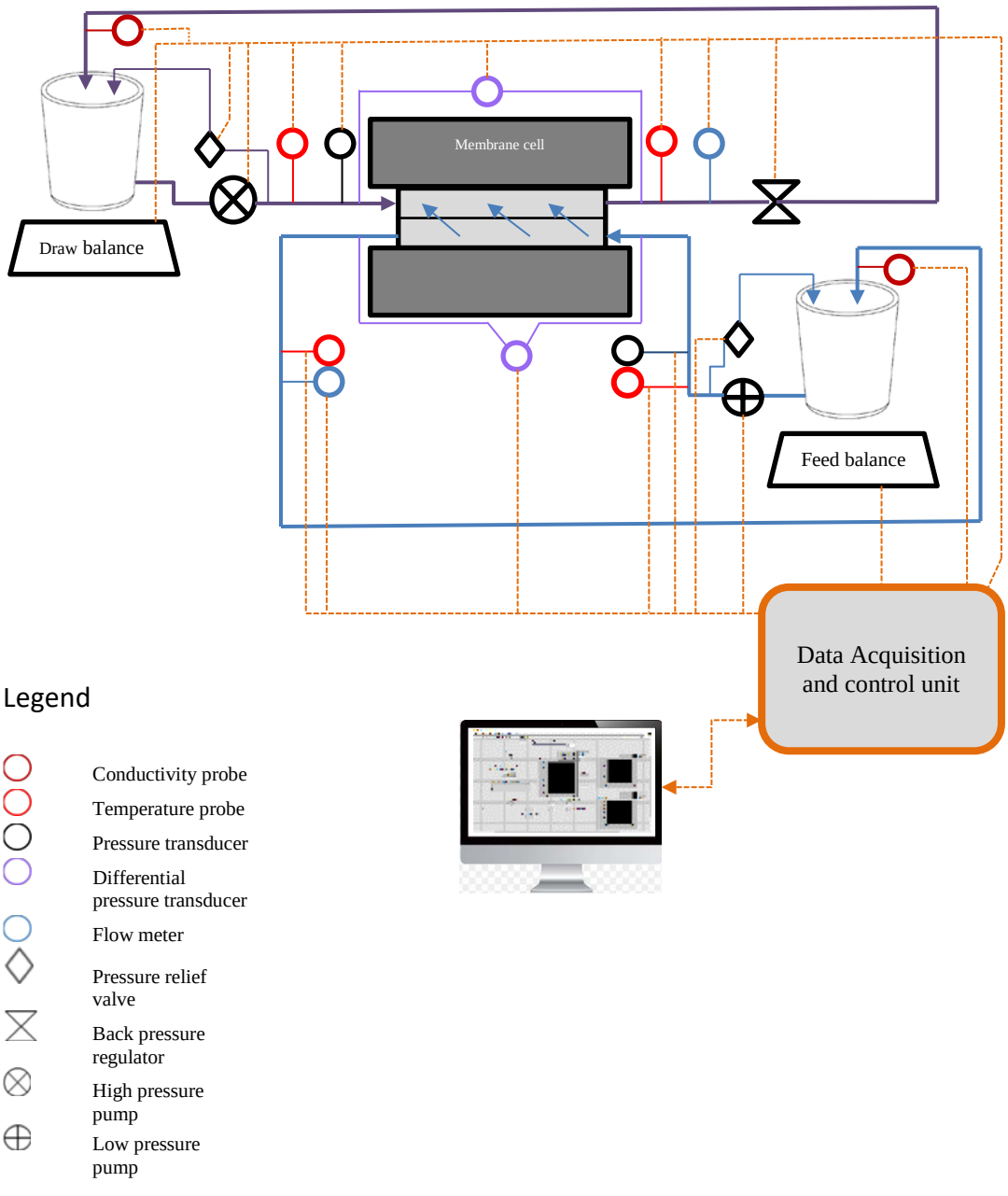

Figure 12: Process flow diagram of PRO setup.

3.2.4 Experimental determination of osmotic pressure

One of the important parameters in the PRO is the osmotic pressure difference between the draw and the feed solution. It is this difference across the membrane which acts as a driving force and is dependent upon the osmotic pressure of the bulk fluids. The osmotic pressure can be calculated roughly using the van't Hoff equation and more accurately using an accurate equation of State. The activity value for the draw solutions was also determined experimentally using a Novasina activity meter and used to calculate the osmotic pressure using Eq. (29). Additionally, the osmotic pressure value was also calculated for different salt solutions from the OLI software and EoS developed by Manzoor et al.[21].

Figure 13: LabMaster osmometer.

4. RESULTS AND DISCUSSION

4.1 Membrane intrinsic characteristics

Pure water permeability coefficient (A) for the two membranes was determined using the CF042D RO unit. It was determined using the water flux values at three different pressures of 2, 6, and 10 bar. The pure water flux value increased with an increase in pressure, as shown below in Fig (14). The value of A is shown in Table (3). For the CTA membrane it is slightly higher than the one reported in the literature [65] whereas for the TFC membrane it is in close agreement with the reported value [73]. The variation in the value for CTA membrane can result due to different flow rate, the flow rate at which experiment was conducted has not been mentioned in the literature.

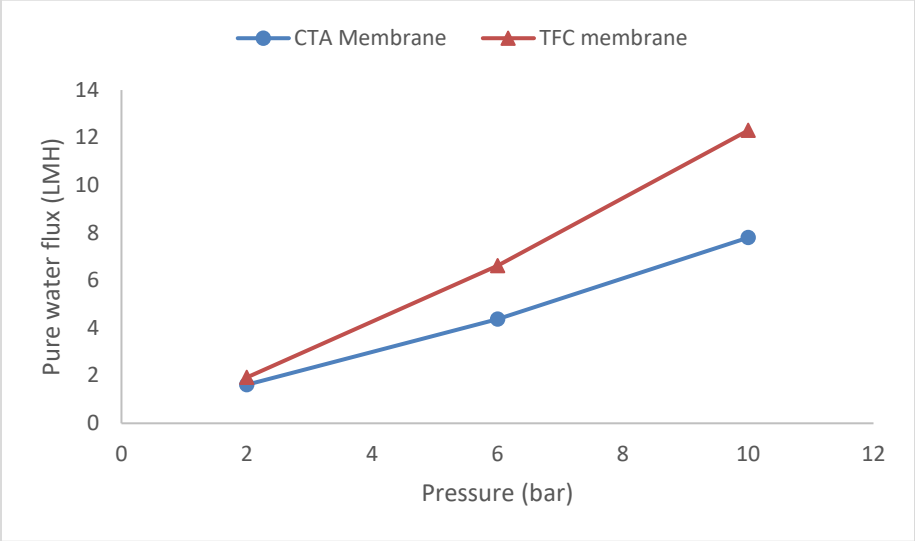

Figure 14: Pure water flux against pressure is plotted for two membrane types. The TFC membrane has higher flux as compared CTA membrane.

Salt permeability coefficient (B) was also determined on the CF042D setup, for determining B the pure water was replaced with 0.1 mM NaCl solution according to the experimental procedure as detailed in Section 3.2.2 of this Thesis. The water flux and salt rejection rate were recorded at 10 bar and the B value was obtained using Eq. (12). The salt rejection rate for both the membranes was more than 95% which is similar to values reported in the literature [40], [73]. The value of salt permeability coefficient for the TFC membrane was found to be higher than the CTA membrane. This is contrary to results reported in the literature where polyamide-based TFC membranes were reported to have lower B value when compared to CTA membranes. However, the results are in accordance with the findings of Straub et al. where they observed an increase in A is accompanied by an increase in B as well when using inorganic salts [30].

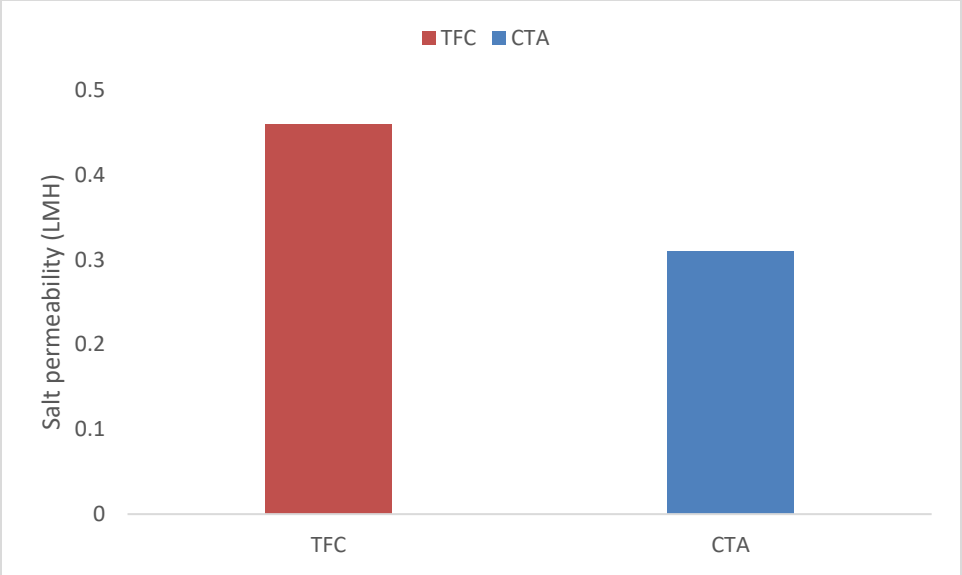

Figure 15: Salt permeability for flat sheet membranes. TFC membrane has a higher value of B when compared to the CTA membrane.

The structural parameter (S) was determined on the CF042A-FO setup. The procedure followed is as detailed in section 3.2.2 of this Thesis, i.e. DI feed and 0.5 M NaCl draw were used. The value of S obtained by the experiments was higher than those reported in the literature for both the membranes. The S value for the TFC membrane was 560 microns, and for the CTA membrane was 1723 microns which are way higher than those reported in the literature for uncompressed FTS membrane but for compressed membrane a high value was reported in a similar study [65]. The structural parameter of TFC and CTA are different as CTA membrane has denser support layer which results in higher tortuosity.

Table 3: Intrinsic characteristics of the CTA and TFC membrane.

Membrane	Pure water permeability, A (L $m^{-2} h^{-1}$ bar)	Salt permeability, B (L $m^{-2} h^{-1}$)	B/A	Salt rejection, R (%)	Structural parameter, S (µm)
CTA (FTS)	0.77	0.31	0.40	96.15	1723
TFC (Toray)	1.29	0.46	0.36	95.42	560

In theory, a good PRO membrane should have high water permeability, low salt permeability, and low structural parameter value. The TFC membranes has higher water permeability but CTA membranes are mechanically stronger for high-pressure operations.

4.2 Membranes PRO performance

The initial performance of the two membranes in PRO mode was performed using the DI feed vs 3M NaCl draw solution. The purpose of these experiments was to set up the base condition and to determine the rupture pressure for both the membranes. Out of the various configurations tested from available spacers and support plate designs, the best result was obtained when two layers of extruded net spacers and Sterlitech SS316 support plate were installed on the feed side and one layer extruded diamond shape spacer was installed on the draw side. The flow rates on both sides were fixed at 40 ml/min. It was observed that the TFC membrane gave a better performance in terms of flux and power density but it can only sustain 35 bar of pressure whereas the CTA membrane was able to operate till 51 bar of pressure under similar conditions. Figure 16 below shows the water flux at different pressure values for both the membranes.

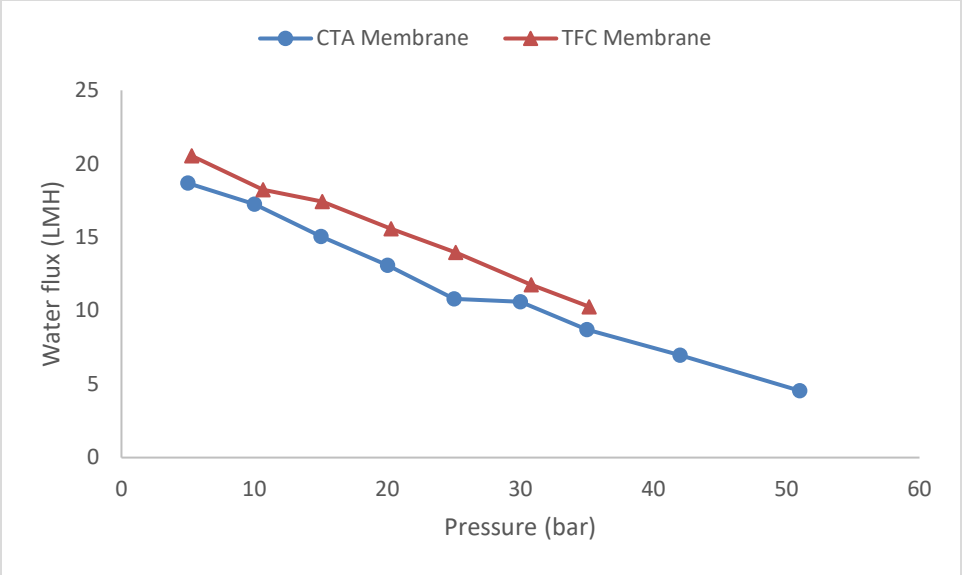

Figure 16: Water flux value for CTA and TFC membrane in PRO mode on using DI feed vs 3M NaCl draw solution. The flux value of the TFC membrane is higher than the CTA membrane but it defaults at 35 bar against CTA which was able to sustain till 51 bar of pressure.

Figure 17 shows the power density versus applied pressure for both CTA and TFC membranes. The maximum power density recorded using the TFC membrane was 10.06 W/m^2 at 30 bar and for the CTA membrane, it was 8.48 W/m^2 at 35 bar. These values are much lower than the theoretical optimum for ideal membranes that is half of the osmotic pressure difference, which is ~ 80 bar in this case. This is because upon increasing the pressure, the internsic membrane properties are changed due to membrane deformation. At high pressure, the active layer pores expand and membrane selectivity decreases, which results in decline of water flux and accordingly power density. This observation was consistent with reported data in the literature [65].

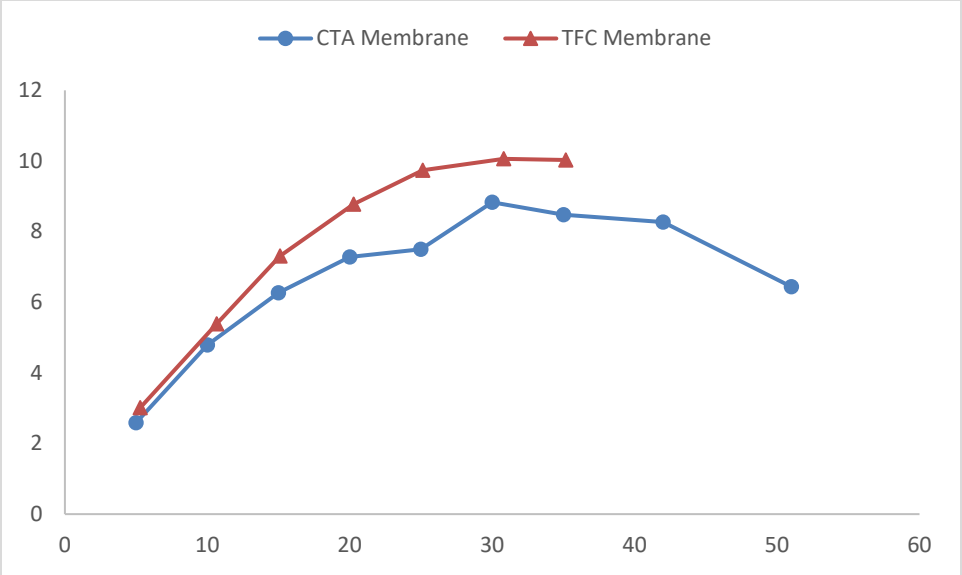

Figure 17: Power density curve for CTA and TFC membrane when using DI feed against the 3M draw.

4.3 Effect of feed salinity on power density output

This series of experiments was performed using 0.6 M NaCl as a feed solution against 3M NaCl draw solution. These experiments were conducted for a pressure range until 30 bar only because as reported earlier, TFC membrane ruptured at a pressure higher than 30 bar. The power density dropped significantly on using the saline feed of 0.6 M. For the CTA membrane the maximum power density reduced by 72% whereas for the TFC membrane there was a drop of 40% in maximum power density when 0.6 M NaCl was used as feed solution representing seawater salinity. The maximum power density of 2.44 W/m^2 for the CTA membrane was recorded at 20 bar whereas for the TFC membrane the maximum power density of 6.0 W/m^2 was recorded at 30 bar. There was a larger drop of power density for the CTA membrane as it has a thicker support layer which results in

more severe ICP. The TFC membrane has thin support layer, which helped to reduce ICP effects.

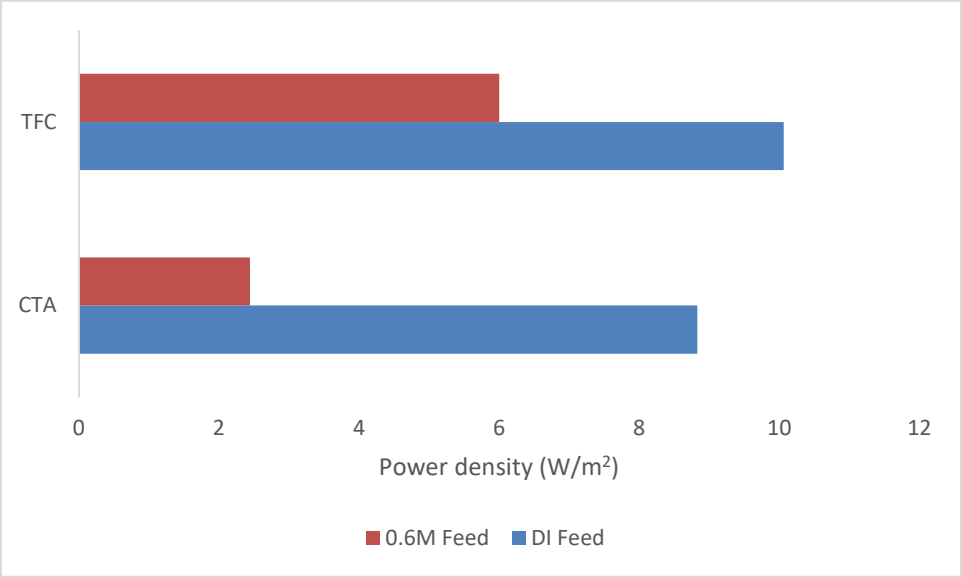

Figure 18: Power density for CTA and TFC membranes on using DI and 0.6 M NaCl as feed solution.

4.4 Effect of feed flow rate on water flux

In these experiments, the effect of feed flow rate on the mass transfer across the CTA membrane was evaluated while keeping the TMP at 5 bar. The draw solution that was used in these experiments was 3M NaCl and its circulation was fixed at 40 ml/min. Two different feed solutions were used, DI water and 0.6 M NaCl and the feed flow was varied from 40 to 200 ml/min. The water flux increased by 15% on circulating DI feed at 200 ml/min from an initial flow rate of 40 ml/min. Similarly, the flux value improved for 0.6 M DI feed by 23 % on running the experiment at a maximum feed flow rate of 200 ml/min.

Figure 19 shows increasing the feed flow rate resulted in slight increase of the flux. The flux for 0.6 M feed was only 9.16 LMH which is very low in comparison to 21.55 LMH for DI feed at 200 ml/min. The increase in flow rate was not very effective in overcoming the ICP effects for the CTA membrane.

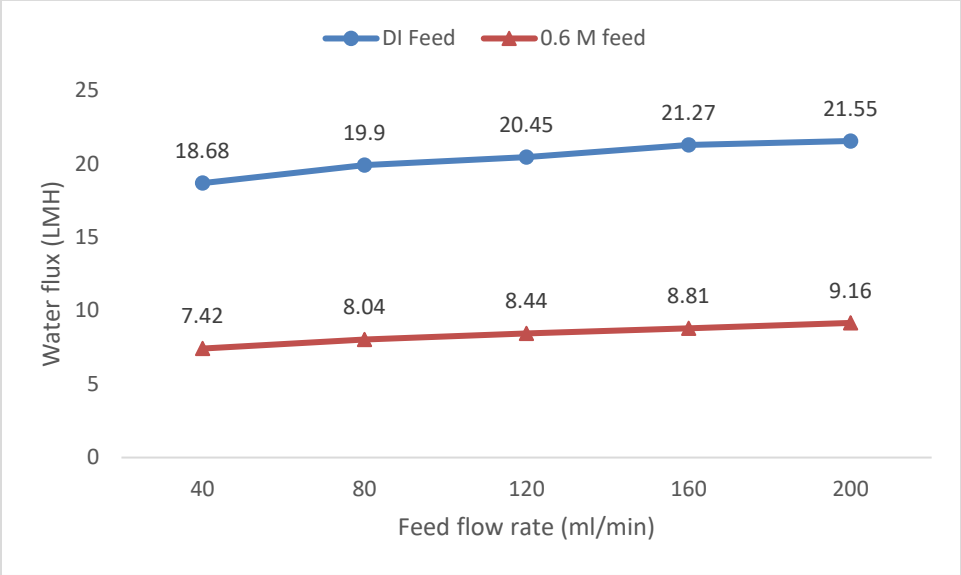

Figure 19: Effect of different feed flow rates on water flux. For these experiments, the pressure and the draw flow rate were kept constant at 5 bar and 40 ml/min respectively.

4.5 Redesigned support plate

It was observed from previous experiments at high concentration of draw solution that the maximum power density is reached at pressures way less than half the osmotic pressure difference. The use of a stainless steel support plate that was provided by the manufacturer did not allow smooth feed flow at high pressure in the draw solution side. By increasing

the pressure, the feed flow decreased and resulted in reduction of transmembrane water flux. We attempted to use multiple layers of tricot spacers but this did not solve the problem. A new support plate was designed and manufactured using the Machine Shop at Texas A&M University. It was 3D printed using Ultimaker tough PLA material and it has 2-mm wide straight channels that allows water to flow smoothly between the spacer and the cell plate surface (Figure 20). The new support plate was used with a single layer of tricot net-type spacer rather than using multiple layers of tricot spacers, which can create entrapment zones where salts accumulate in addition of not being efficient in enhancing feed flow. .

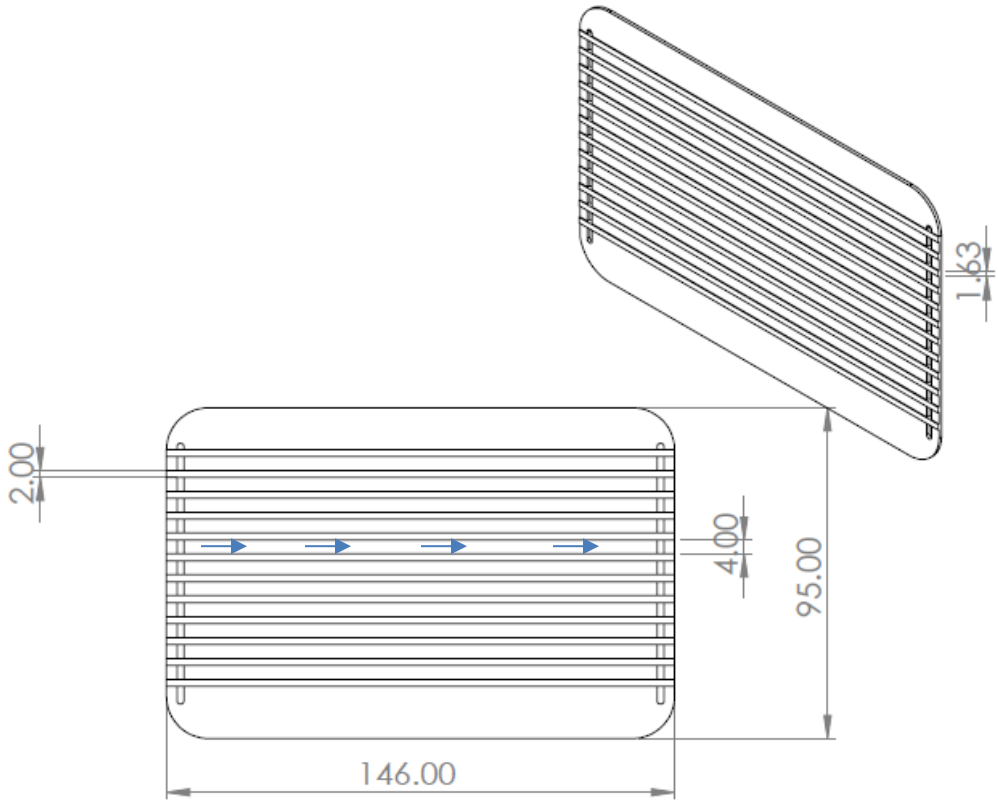

Figure 20: 2D view of the in-house fabricated support plate with straight flow channels. The blue arrow signifies the direction of feed flow on the support plate.

It can be observed from Figure 2 below that on installing the new support plate along with the closely-knit tricot spacer, the CTA membrane performance improved by over 100 percent. The threshold power density value of 5 W/m^2 was obtained at 5 bar and on increasing the TMP the power density reached a maximum of 19.49 W/m^2 at 30 bar. The values obtained for the CTA membrane during this experiment were in close agreement with the values reported by Madsen et al. [65] in their study for the FTS CTA membrane. For these experiments, the feed and the draw were circulated at a flow rate of 40 ml/min.

The experiment was discontinued beyond 30 bar due to the mechanical deformation of the PLC support plate.

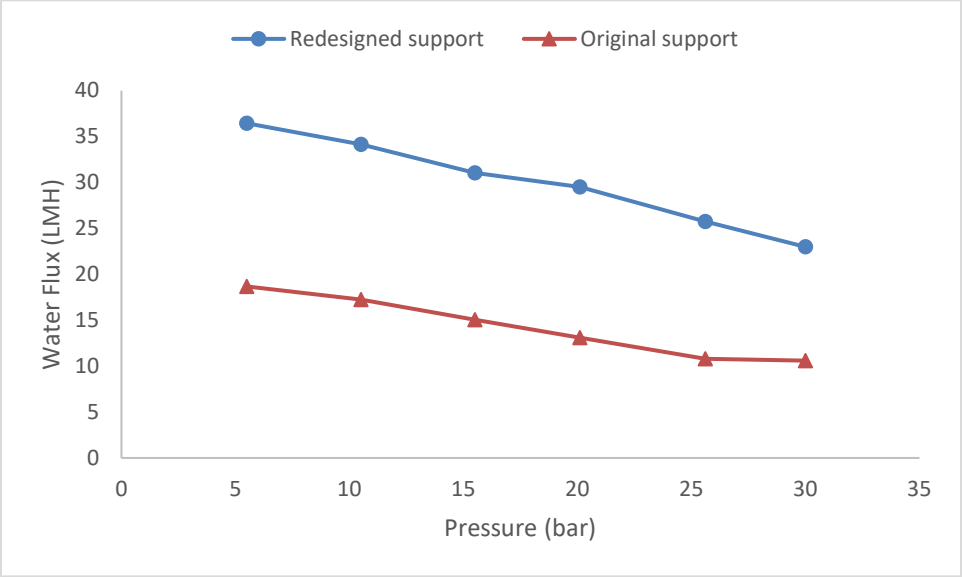

Figure 21: Increased water flux for the CTA membrane on installing the re-designed support plate along with the single layer of tricot spacer.

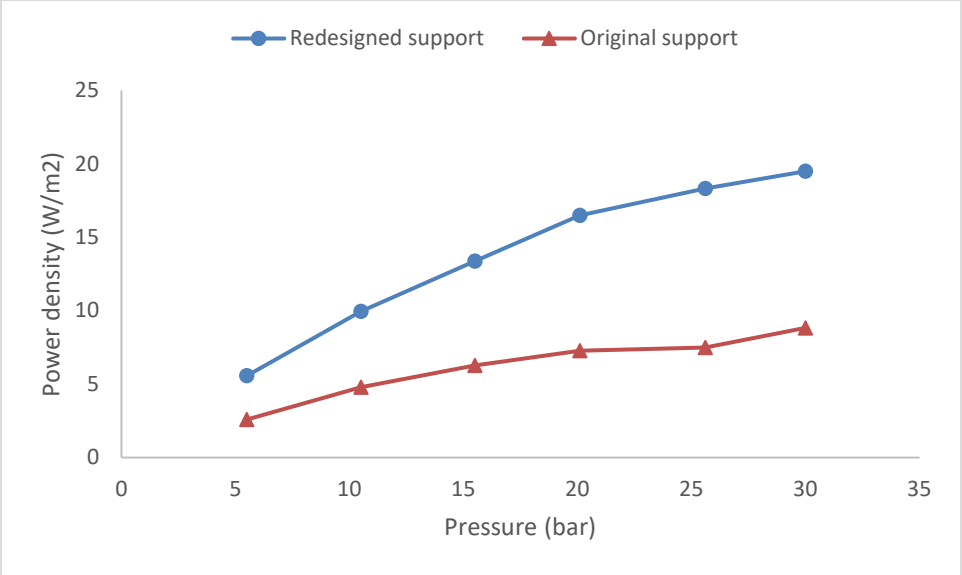

Figure 22: Increased power density for the CTA membrane on installing the re-designed support plate along with the single layer of tricot spacer. The power density of 19 W/m2 was achieved at TMP of 30 bar.

4.5 Osmotic pressure measurement

The activity of different NaCl solutions was measured experimentally using the Novasina activity meter. The experimental value was then used in Eq. (28) for obtaining the osmotic pressures of solutions used in this research experimentally. The osmotic pressure was also calculated using the OLI Systems, Inc. (Morris Plains, NJ) and equation of state developed by Manzoor et al. [21]. These values were also compared to the values reported in the literature by Madsen et al. [65] as shown in Figure 22. As can be seen from Figure 22 the value of osmotic pressure determined by various methods are all in very close agreement over the whole range of salt concentrations.

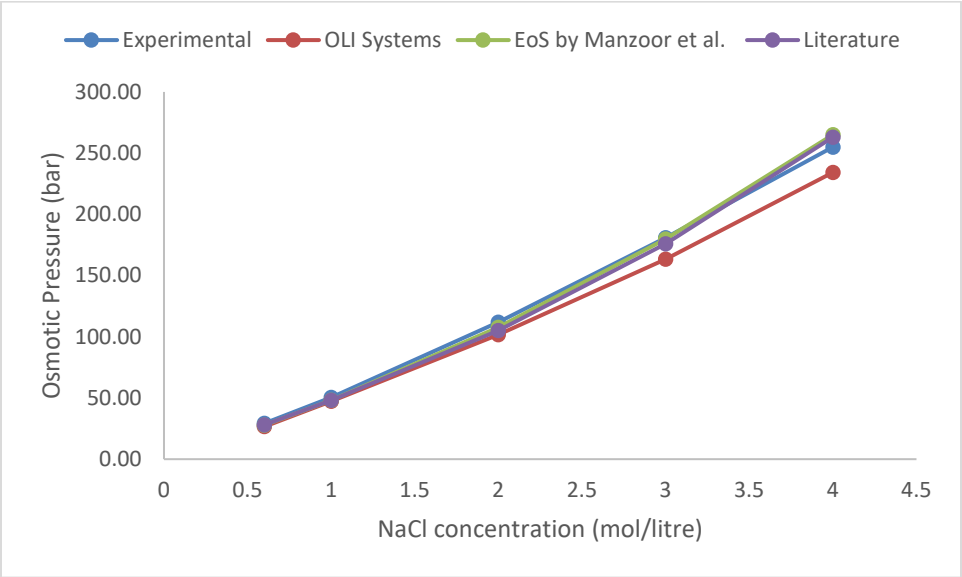

Figure 23: Osmotic Pressure determined experimentally using activity model, OLI software, and EoS developed by Manzoor et al.

5. CONCLUSIONS AND RECOMMENDATIONS

The aim of this research work was to experimentally analyze the performance of PRO technology for high salinity draw solutions using CTA and TFC membranes by varying the process conditions. The process parameters investigated were the feed salinity, feed flow rate, and different configuration and design of the spacers. Also, the intrinsic characteristics of the membrane and osmotic pressure of the draw solution were determined experimentally.

Based on the experimental results, the following conclusions can be made:

- TFC membrane has higher power production potential for PRO but is limited to low-pressure operations.
- CTA membranes have higher mechanical strength than TFC membranes exhibited high performance on using properly designed spacers and support plate.
- The effect of the ICP due to the use of saline feed was not successfully negated even on circulating the feed at the higher flow rate.
- The membranes was mechanically deformed at high pressure due to both rupturing as well as distortion of the selective layer pores.

The work performed in this study utilized NaCl synthetic solutions. The future investigation into PRO performance can be done using the actual brines found in nature and industry as detailed in section 2.4.1. Also, the new generation of feed spacers effect on the PRO performance can be studied with the help of CFD tools. A 3D hydrodynamic

model can help in predicting the flow and mass transfer around the membrane on using particular spacer design under different experimental conditions.

REFERENCES

[1] O. Edenhofer *et al., IPCC, 2011: Summary for Policymakers. In: IPCC Special Report on Renewable Energy Sources and Climate Change Mitigation*. 2011.

[2] International Energy Agency (IEA), "CO_2 Emissions from Fuel Combustion 2014," *Int. energy agency*, vol. 1, no. 1, p. 134, 2014, doi: 10.1787/co2_fuel-2014-en.

[3] C. Kim, S. Lee, H. K. Shon, M. Elimelech, and S. Hong, "Boron transport in forward osmosis: Measurements, mechanisms, and comparison with reverse osmosis," *J. Memb. Sci.*, vol. 419–420, pp. 42–48, 2012, doi: 10.1016/j.memsci.2012.06.042.

[4] T. Y. Cath, A. E. Childress, and M. Elimelech, "Forward osmosis: Principles, applications, and recent developments," *J. Memb. Sci.*, vol. 281, no. 1–2, pp. 70–87, 2006, doi: 10.1016/j.memsci.2006.05.048.

[5] A. C. Mecha, "Applications of Reverse and Forward Osmosis Processes in Wastewater Treatment: Evaluation of Membrane Fouling," in *Osmotically Driven Membrane Processes - Approach, Development and Current Status*, InTech, 2018.

[6] S. Zhang, G. Han, X. Li, C. Wan, and T. S. Chung, *Pressure retarded osmosis: Fundamentals*. 2016.

[7] A. Achilli and K. L. Hickenbottom, *Pressure retarded osmosis: Applications*. Elsevier Ltd., 2016.

[8] K. L. Lee, R. W. Baker, and H. K. Lonsdale, "Membranes for power generation by pressure-retarded osmosis," *J. Memb. Sci.*, vol. 8, no. 2, pp. 141–171, 1981, doi:

10.1016/S0376-7388(00)82088-8.

[9] R. Pattle, “Production of Electric Power by mixing Fresh and Salt Water in the Hydroelectric Pile,” *Nature*, vol. 174, no. 1953, p. 1954, 1954, [Online]. Available: https://doi.org/10.1038/174660a0.

[10] S. Loeb, “Production of energy from concentrated brines by pressure-retarded osmosis. I. Preliminary technical and economic correlations,” *J. Memb. Sci.*, vol. 1, no. C, pp. 49–63, 1976, doi: 10.1016/S0376-7388(00)82257-7.

[11] S. Loeb, F. Van Hessen, and D. Shahaf, “Production of energy from concentrated brines by pressure-retarded osmosis. II. Experimental results and projected energy costs,” *J. Memb. Sci.*, vol. 1, no. C, pp. 249–269, 1976, doi: 10.1016/S0376-7388(00)82271-1.

[12] S. Loeb and R. S. Norman, “Osmotic power plants,” *Sci. Mag.*, vol. 189, pp. 654–655, 1975, [Online]. Available: 10.1126/science.189.4203.654.

[13] R. S. Norman, “Water Salination : A Source of Energy Author (s): Richard S . Norman Published by : American Association for the Advancement of Science Stable URL : http://www.jstor.org/stable/1739781 digitize , preserve and extend access to Science,” *Science (80-.).*, vol. 186, no. 4161, pp. 350–352, 1974.

[14] G. D. Mehta and S. Loeb, “Internal polarization in the porous substructure of a semipermeable membrane under pressure-retarded osmosis,” *J. Memb. Sci.*, vol. 4, no. C, pp. 261–265, 1978, doi: 10.1016/S0376-7388(00)83301-3.

[15] S. Loeb, T. Honda, and M. Reali, “Comparative mechanical efficiency of several plant configurations using a pressure-retarded osmosis energy converter,” *J. Memb.*

Sci., vol. 51, no. 3, pp. 323–335, 1990, doi: 10.1016/S0376-7388(00)80354-3.

[16] M. Reali, G. Dassie, and G. Jonsson, “Computation of salt concentration profiles in the porous substrate of anisotropic membranes under steady pressure-retarded-osmosis conditions,” *J. Memb. Sci.*, vol. 48, no. 2–3, pp. 181–201, 1990, doi: 10.1016/0376-7388(90)85004-5.

[17] S. Loeb, “Energy production at the Dead Sea by pressure-retarded osmosis: Challenge or chimera?,” *Desalination*, vol. 120, no. 3, pp. 247–262, 1998, doi: 10.1016/S0011-9164(98)00222-7.

[18] S. Loeb, “One hundred and thirty benign and renewable megawatts from Great Salt Lake? The possibilities of hydroelectric power by pressure-retarded osmosis,” *Desalination*, vol. 141, no. 1, pp. 85–91, 2001, doi: 10.1016/S0011-9164(01)00392-7.

[19] S. Loeb, “Large-scale power production by pressure-retarded osmosis, using river water and sea water passing through spiral modules,” *Desalination*, vol. 143, no. 2, pp. 115–122, 2002, doi: 10.1016/S0011-9164(02)00233-3.

[20] A. P. Straub, N. Y. Yip, and M. Elimelech, “Raising the Bar: Increased Hydraulic Pressure Allows Unprecedented High Power Densities in Pressure-Retarded Osmosis,” *Environ. Sci. Technol. Lett.*, vol. 1, no. 1, pp. 55–59, 2013, doi: 10.1021/ez400117d.

[21] H. Manzoor, M. A. Selam, F. Bin Abdur Rahman, S. Adham, M. Castier, and A. Abdel-Wahab, “A tool for assessing the scalability of pressure-retarded osmosis (PRO) membranes,” *Renew. Energy*, vol. 149, pp. 987–999, 2020, doi:

10.1016/j.renene.2019.10.098.

[22] N. Bajraktari, C. Hélix-Nielsen, and H. T. Madsen, “Pressure retarded osmosis from hypersaline sources — A review,” *Desalination*, vol. 413, pp. 65–85, 2017, doi: 10.1016/j.desal.2017.02.017.

[23] H. Kim, J. S. Choi, and S. Lee, “Pressure retarded osmosis for energy production: Membrane materials and operating conditions,” *Water Sci. Technol.*, vol. 65, no. 10, pp. 1789–1794, 2012, doi: 10.2166/wst.2012.025.

[24] M. Li, “Analysis and Optimization of Pressure Retarded Osmosisfor Power Generation,” *AICHE J.*, vol. 61, no. 3, pp. 857–866, 2015, doi: 10.1002/aic.

[25] A. Tamburini, F. Giacalone, A. Cipollina, F. Grisafi, G. Vella, and G. Micale, “Pressure retarded osmosis: A membrane process for environmental sustainability,” *Chem. Eng. Trans.*, vol. 47, no. March, pp. 355–360, 2016, doi: 10.3303/CET1647060.

[26] N. Y. Yip *et al.*, “Thin-film composite pressure retarded osmosis membranes for sustainable power generation from salinity gradients,” *Environ. Sci. Technol.*, vol. 45, no. 10, pp. 4360–4369, 2011, doi: 10.1021/es104325z.

[27] F. Helfer, C. Lemckert, and Y. G. Anissimov, “Osmotic power with Pressure Retarded Osmosis: Theory, performance and trends - A review,” *J. Memb. Sci.*, vol. 453, pp. 337–358, 2014, doi: 10.1016/j.memsci.2013.10.053.

[28] A. Achilli, T. Y. Cath, and A. E. Childress, “Power generation with pressure retarded osmosis: An experimental and theoretical investigation,” *J. Memb. Sci.*, vol. 343, no. 1–2, pp. 42–52, 2009, doi: 10.1016/j.memsci.2009.07.006.

[29] K. Touati, C. Hänel, F. Tadeo, and T. Schiestel, “Effect of the feed and draw solution temperatures on PRO performance: Theoretical and experimental study,” *Desalination*, vol. 365, pp. 182–195, 2015, doi: 10.1016/j.desal.2015.02.016.

[30] A. P. Straub, A. Deshmukh, and M. Elimelech, “Pressure-retarded osmosis for power generation from salinity gradients: Is it viable?,” *Energy Environ. Sci.*, vol. 9, no. 1, pp. 31–48, 2016, doi: 10.1039/c5ee02985f.

[31] N. Y. Yip and M. Elimelech, “Performance limiting effects in power generation from salinity gradients by pressure retarded osmosis,” *Environ. Sci. Technol.*, vol. 45, no. 23, pp. 10273–10282, 2011, doi: 10.1021/es203197e.

[32] S. Kim, “Scale-up of osmotic membrane bioreactors by modeling salt accumulation and draw solution dilution using hollow-fiber membrane characteristics and operation conditions,” *Bioresour. Technol.*, vol. 165, pp. 88–95, 2014, doi: 10.1016/j.biortech.2014.03.101.

[33] S. H. Park, B. Park, H. K. Shon, and S. Kim, “Modeling full-scale osmotic membrane bioreactor systems with high sludge retention and low salt concentration factor for wastewater reclamation,” *Bioresour. Technol.*, vol. 190, pp. 508–515, 2015, doi: 10.1016/j.biortech.2015.03.094.

[34] G. Han, S. Zhang, X. Li, and T. S. Chung, “Progress in pressure retarded osmosis (PRO) membranes for osmotic power generation,” *Prog. Polym. Sci.*, vol. 51, pp. 1–27, 2014, doi: 10.1016/j.progpolymsci.2015.04.005.

[35] K. L. Hickenbottom, J. Vanneste, M. Elimelech, and T. Y. Cath, “Assessing the current state of commercially available membranes and spacers for energy

production with pressure retarded osmosis," *Desalination*, vol. 389, pp. 108–118, 2016, doi: 10.1016/j.desal.2015.09.029.

[36] Y. C. Kim and M. Elimelech, "Adverse impact of feed channel spacers on the performance of pressure retarded osmosis," *Environ. Sci. Technol.*, vol. 46, no. 8, pp. 4673–4681, 2012, doi: 10.1021/es3002597.

[37] Q. She, D. Hou, J. Liu, K. H. Tan, and C. Y. Tang, "Effect of feed spacer induced membrane deformation on the performance of pressure retarded osmosis (PRO): Implications for PRO process operation," *J. Memb. Sci.*, vol. 445, pp. 170–182, 2013, doi: 10.1016/j.memsci.2013.05.061.

[38] J. Kim, B. Kim, D. Inhyuk Kim, and S. Hong, "Evaluation of apparent membrane performance parameters in pressure retarded osmosis processes under varying draw pressures and with draw solutions containing organics," *J. Memb. Sci.*, vol. 493, pp. 636–644, 2015, doi: 10.1016/j.memsci.2015.07.035.

[39] J. Lee and S. Kim, "Predicting power density of pressure retarded osmosis (PRO) membranes using a new characterization method based on a single PRO test," *Desalination*, vol. 389, pp. 224–234, 2016, doi: 10.1016/j.desal.2016.01.026.

[40] T. Y. Cath *et al.*, "Standard Methodology for Evaluating Membrane Performance in Osmotically Driven Membrane Processes," *Desalination*, vol. 312, pp. 31–38, 2013, doi: 10.1016/j.desal.2012.07.005.

[41] A. Tiraferri, N. Y. Yip, A. P. Straub, S. Romero-Vargas Castrillon, and M. Elimelech, "A method for the simultaneous determination of transport and structural parameters of forward osmosis membranes," *J. Memb. Sci.*, vol. 444, pp.

523–538, 2013, doi: 10.1016/j.memsci.2013.05.023.

[42] R. R. Gonzales, M. J. Park, L. Tijing, D. S. Han, S. Phuntsho, and H. K. Shon, “Modification of nanofiber support layer for thin film composite forward osmosis membranes via layer-by-layer polyelectrolyte deposition,” *Membranes (Basel).*, vol. 8, no. 3, pp. 1–15, 2018, doi: 10.3390/membranes8030070.

[43] E. Nagy, “A general, resistance-in-series, salt- and water flux models for forward osmosis and pressure-retarded osmosis for energy generation,” *J. Memb. Sci.*, vol. 460, pp. 71–81, 2014, doi: 10.1016/j.memsci.2014.02.021.

[44] S. Chou, R. Wang, L. Shi, Q. She, C. Tang, and A. G. Fane, “Thin-film composite hollow fiber membranes for pressure retarded osmosis (PRO) process with high power density,” *J. Memb. Sci.*, vol. 389, pp. 25–33, 2012, doi: 10.1016/j.memsci.2011.10.002.

[45] B. D. Coday, D. M. Heil, P. Xu, and T. Y. Cath, “Effects of transmembrane hydraulic pressure on performance of forward osmosis membranes,” *Environ. Sci. Technol.*, vol. 47, no. 5, pp. 2386–2393, 2013, doi: 10.1021/es304519p.

[46] C. P. Koutsou, S. G. Yiantsios, and A. J. Karabelas, “A numerical and experimental study of mass transfer in spacer-filled channels: Effects of spacer geometrical characteristics and Schmidt number,” *J. Memb. Sci.*, vol. 326, no. 1, pp. 234–251, 2009, doi: 10.1016/j.memsci.2008.10.007.

[47] Y. Xu, X. Peng, C. Y. Tang, Q. S. Fu, and S. Nie, “Effect of draw solution concentration and operating conditions on forward osmosis and pressure retarded osmosis performance in a spiral wound module,” *J. Memb. Sci.*, vol. 348, no. 1–2,

pp. 298–309, 2010, doi: 10.1016/j.memsci.2009.11.013.

[48] Q. She, X. Jin, and C. Y. Tang, “Osmotic power production from salinity gradient resource by pressure retarded osmosis: Effects of operating conditions and reverse solute diffusion,” *J. Memb. Sci.*, vol. 401–402, pp. 262–273, 2012, doi: 10.1016/j.memsci.2012.02.014.

[49] M. Kelada, “Global Potential of Hypersalinity Osmotic Power,” no. Table 1, pp. 1–12, 2010.

[50] G. L. Wick and J. D. Isaacs, “Salt domes: Is there more energy available from their salt than from their oil?,” *Science (80-.).*, vol. 199, no. 4336, pp. 1436–1437, 1978, doi: 10.1126/science.199.4336.1436.

[51] G. L. Wick, “Power from salinity gradients,” *Energy*, vol. 3, no. 1, pp. 95–100, 1978, doi: 10.1016/0360-5442(78)90059-2.

[52] W. G. Williams, G. L. Wick, and I. J.D., “Mineral Salt : A Source of Costly Energy ?,” *Science (80-.).*, vol. 203, no. JANUARY, pp. 1978–1980, 1979.

[53] H. T. Madsen, S. S. Nissen, and E. G. Søgaard, “Theoretical framework for energy analysis of hypersaline pressure retarded osmosis,” *Chem. Eng. Sci.*, vol. 139, pp. 211–220, 2016, doi: 10.1016/j.ces.2015.09.018.

[54] H. Sakai *et al.*, “Energy recovery by PRO in sea water desalination plant,” *Desalination*, vol. 389, pp. 52–57, 2016, doi: 10.1016/j.desal.2016.01.025.

[55] E. J. Sullivan Graham, A. C. Jakle, and F. D. Martin, “Reuse of oil and gas produced water in south-eastern New Mexico: resource assessment, treatment processes, and policy,” *Water Int.*, vol. 40, no. 5–6, pp. 809–823, 2015, doi:

10.1080/02508060.2015.1096126.

[56] G. P. Thiel and J. H. Lienhard V, “Treating produced water from hydraulic fracturing: Composition effects on scale formation and desalination system selection,” *Desalination*, vol. 346, pp. 54–69, 2014, doi: 10.1016/j.desal.2014.05.001.

[57] G. P. Thiel, E. W. Tow, L. D. Banchik, H. W. Chung, and J. H. Lienhard V, “Energy consumption in desalinating produced water from shale oil and gas extraction,” *Desalination*, vol. 366, pp. 94–112, 2015, doi: 10.1016/j.desal.2014.12.038.

[58] K. Guerra, K. Dahm, and S. Dundorf, “Oil and Gas Produced Water Management and Beneficial Use in the Western United States,” *U.S. Dep. Inter. Bur. Reclamation, Manag. Water West*, no. 157, p. 129, 2011, doi: 3180.

[59] E. T. Igunnu and G. Z. Chen, “Produced water treatment technologies,” *Int. J. Low-Carbon Technol.*, vol. 9, no. 3, pp. 157–177, 2012, doi: 10.1093/ijlct/cts049.

[60] A. E. Larson, E. A. Johnson, and J. H. Nelson, “Survival of Listeria monocytogenes in commercial cheese brines,” *J. Dairy Sci.*, vol. 82, no. 9, pp. 1860–1868, 1999, doi: 10.3168/jds.S0022-0302(99)75419-6.

[61] M. Kubo, J. Hiroe, M. Murakami, H. Fukami, and T. Tachiki, “Treatment of hypersaline-containing wastewater with salt-tolerant microorganisms,” *J. Biosci. Bioeng.*, vol. 91, no. 2, pp. 222–224, 2001, doi: 10.1016/S1389-1723(01)80070-0.

[62] W. Suntornsuk, “Yeast cultivation in lettuce brine,” *World J. Microbiol. Biotechnol.*, vol. 16, no. 8–9, pp. 815–818, 2000, doi: 10.1023/A:1008926700452.

[63] D. Xu, S. Wang, J. Zhang, X. Tang, Y. Guo, and C. Huang, “Supercritical water

oxidation of a pesticide wastewater," *Chem. Eng. Res. Des.*, vol. 94, no. August, pp. 396–406, 2015, doi: 10.1016/j.cherd.2014.08.016.

[64] M. Turek, B. Bandura, and P. Dydo, "Power production from coal-mine brine utilizing reversed electrodialysis," *Desalination*, vol. 221, no. 1–3, pp. 462–466, 2008, doi: 10.1016/j.desal.2007.01.106.

[65] H. T. Madsen, S. S. Nissen, J. Muff, and E. G. Søgaard, "Pressure retarded osmosis from hypersaline solutions: Investigating commercial FO membranes at high pressures," *Desalination*, vol. 420, no. March, pp. 183–190, 2017, doi: 10.1016/j.desal.2017.06.028.

[66] K. L. Hickenbottom, J. Vanneste, and T. Y. Cath, "Assessment of alternative draw solutions for optimized performance of a closed-loop osmotic heat engine," *J. Memb. Sci.*, vol. 504, pp. 162–175, 2016, doi: 10.1016/j.memsci.2016.01.001.

[67] S. Adhikary, M. S. Islam, K. Touati, S. Sultana, A. S. Ramamurthy, and M. S. Rahaman, "Increased power density with low salt flux using organic draw solutions for pressure-retarded osmosis at elevated temperatures," *Desalination*, vol. 484, no. March, p. 114420, 2020, doi: 10.1016/j.desal.2020.114420.

[68] N. Y. Yip and M. Elimelech, "Thermodynamic and energy efficiency analysis of power generation from natural salinity gradients by pressure retarded osmosis," *Environ. Sci. Technol.*, vol. 46, no. 9, pp. 5230–5239, 2012, doi: 10.1021/es300060m.

[69] S. Lin, A. P. Straub, and M. Elimelech, "Thermodynamic limits of extractable energy by pressure retarded osmosis," *Energy Environ. Sci.*, vol. 7, no. 8, pp. 2706–

2714, 2014, doi: 10.1039/c4ee01020e.

[70] A. D. Wilson and F. F. Stewart, “Deriving osmotic pressures of draw solutes used in osmotically driven membrane processes,” *J. Memb. Sci.*, vol. 431, pp. 205–211, 2013, doi: 10.1016/j.memsci.2012.12.042.

[71] K. S. Pitzer, J. C. Peiper, and R. H. Busey, “Thermodynamic Properties of Aqueous Sodium Chloride Solutions,” *J. Phys. Chem. Ref. Data*, vol. 13, no. 1, pp. 1–102, 1984, doi: 10.1063/1.555709.

[72] J. Newman and K. Thomas-Aleya, *Electrochemical Systems*, 3rd ed. John Wiley & Sons, 2004.

[73] R. R. Gonzales *et al.*, “Melamine-based covalent organic framework-incorporated thin film nanocomposite membrane for enhanced osmotic power generation,” *Desalination*, vol. 459, no. March, pp. 10–19, 2019, doi: 10.1016/j.desal.2019.02.013.